

# Out-of-Distribution Detection with Distance Guarantee in Deep Generative Models

Yufeng Zhang<sup>\*a</sup>, Wanwei Liu<sup>†b</sup>, Zhenbang Chen<sup>‡b</sup>, Ji Wang<sup>§b</sup>, Zhiming Liu<sup>¶c</sup>, Kenli Li<sup>||a</sup>, Hongmei Wei<sup>\*\*d</sup>, and Zuoning Chen<sup>††e</sup>

<sup>a</sup>College of Information Science and Engineering, Hunan University, Changsha, China

<sup>b</sup>College of Computer Science, National University of Defense Technology, Changsha, China

<sup>c</sup>Southwest University, Chongqing, China

<sup>d</sup>Department of Compute Science & Engineering, Shanghai Jiao Tong University, Shanghai, China

<sup>e</sup>National Research Center of Parallel Computer Engineering and Technology, China

## Abstract

Recent research has shown that it is challenging to detect out-of-distribution (OOD) data in deep generative models including flow-based models and variational autoencoders (VAEs). In this paper, we prove a theorem that, for a well-trained flow-based model, the distance between the distribution of representations of an OOD dataset and prior can be large enough, as long as the distance between the distributions of the training dataset and the OOD dataset is large enough. Furthermore, our observation shows that, for flow-based model and VAE with factorized prior, the representations of OOD datasets are more correlated than that of the training dataset. Based on our theorem and observation, we propose detecting OOD data according to the total correlation of representations in flow-based model and VAE. Experimental results show that our method can achieve nearly 100% AUROC for all the widely used benchmarks and has robustness against data manipulation. While the state-of-the-art method performs not better than random guessing for challenging problems and can be fooled by data manipulation in almost all cases.

## 1 Introduction

Generally, a generative model  $p_{\theta}(\mathbf{x})$  with parameters  $\theta$  is trained to approximate an unknown distribution  $p^*(\mathbf{x})$ , given that the training inputs are drawn independently from  $p^*$ . Modern deep generative models (DGM) including variational auto-encoders (VAE) [26], generative adversarial networks (GAN) [19], auto-regressive models [45, 41] and flow-based invertible models [27, 16] have been developed and applied in many fields such as visual recognition and generation [7, 27], speech generation [36] and natural language processing [33]. Specially, VAE, auto-regressive model and flow-based model have drawn interests of researchers since they can offer explicit marginal likelihood of data points.

Recent research shows that DGMs are not capable of distinguishing OOD data from training data (or in-distribution (InD) data) according to the model likelihood [34, 42, 13, 43, 35]. For example, flow-based models including Glow [27, 16] may assign a higher likelihood for SVHN (MNIST) when trained on CIFAR10 (FashionMNIST). This counterintuitive phenomenon also occurs in VAE [26] and auto-regressive models [45, 41]. PixelCNN [34]. However, *we cannot sample out data similar to OOD dataset*.

Another similar phenomenon is observed in the class conditional flow-based model, which contains a Gaussian Mixture Model (GMM) on the top layer with one Gaussian for each class [18]. For example, class conditional Glow only achieves 82.8% classification precision on FashionMNIST. This means that one component may assign higher likelihoods for the inputs of other classes. However, *we always sample out images of the correct classes from the GMM*.

Some researchers conjecture that these counterintuitive phenomena stem from the distinction of high probability density regions and the typical set of the model distribution [35, 13]. For example, the typical set of  $d$ -dimensional isotropic Gaussian is an annulus with a radius of  $\sqrt{d}$  [46]. When sampling from the Gaussian, it is likely to obtain points in the typical set, rather than the highest density region (*i.e.* the center). Nalisnick et al. propose using typicality test

---

\*Corresponding author: yuffonzhang@163.com

†wwliu@nudt.edu.cn

‡zbchen@nudt.edu.cn

§wj@nudt.edu.cn

¶zhimingliu88@swu.edu.cn

||Corresponding author: lkl@hnu.edu.cn

\*\*wei-hong-mei@sjtu.edu.cn

††chenzuoning@vip.163.com

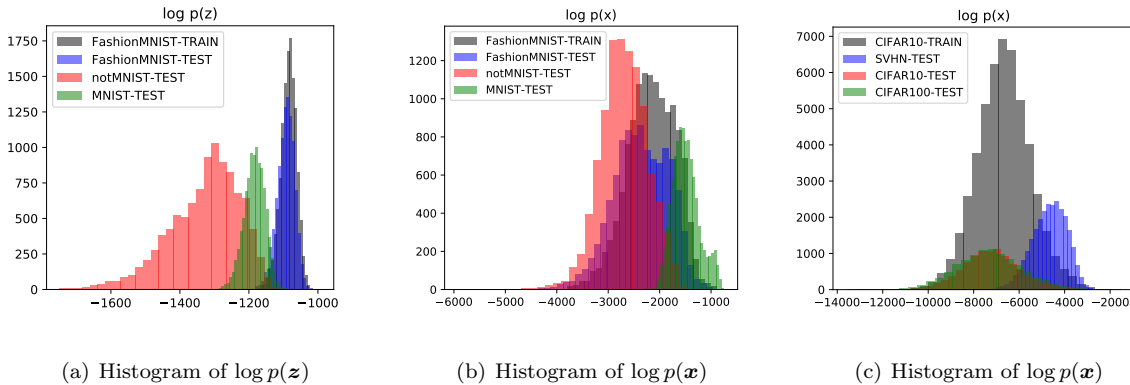


Figure 1: Glow trained on FashionMNIST (CIFAR10) and tested on FashionMNIST/MNIST (CIFAR100/SVHN).

(Ty-test in short) to detect OOD data and achieve state-of-the-art results [35]. However, when the likelihood distribution of InD and OOD datasets coincide, any likelihood- (typicality-) based methods would fail.

We start our research from the sampling process. Flow-based model is bijection mapping every input  $\mathbf{x}$  to unique  $\mathbf{z} = f(\mathbf{x})$  in the latent space. We should ask why we cannot sample out the representations of OOD data from prior. In this paper, we reveal that the reason is the divergence between the distribution of representations of OOD data and prior. We prove a theorem that, for a well-trained flow-based model, the distance between the distribution of representations of OOD dataset  $q_Z$  and the prior  $p_r$  can be large enough, as long as the distance between distributions of InD and OOD datasets is large enough.

Our theorem also prompts us to detect OOD data according to the divergence between the distribution of representations and prior. In this paper, we propose using the total correlation of representations as the criterion for OOD detection. We select total correlation for two reasons. Firstly, flow-based model preserves  $(h, \phi)$ -divergence, which includes the KullbackLeibler (KL) divergence defining total correlation. Secondly, we have observed that, for flow-based models and VAE with factorized prior, the representations of OOD datasets are more correlated than that of InD dataset for all model-dataset pairs.

The contributions of this paper are as follows:

1. We prove that, for a well-trained flow-based model, the distance between the distribution of representations of OOD dataset and prior can be large enough, as long as the distance between the distributions of InD and OOD datasets is large enough. This explains why we cannot sample out new samples like OOD data from flow-based model.
2. We propose detecting OOD data according to the total correlation based on fitted Gaussian against the prior in flow-based model and VAE.
3. The experimental results show that our method can achieve nearly 100% AUROC for all the problems encountered in the experiments and is robust against data manipulation. While the state-of-the-art method is not better than random guessing for challenging problems and can be fooled by data manipulation in almost all cases.

The remainder of this paper is organized as follows. Section 2 discusses the problem of interest. Section 3 gives out the theoretical analysis. Section 4 shows the details of our OOD detection method. Section 5 reports the experimental results. Section 6 discusses the related work. Finally, Section 7 concludes.

## 2 Problem of Interest

### 2.1 Background

**Flow-based generative models** construct diffeomorphism  $f$  from visible space  $\mathcal{X}$  to latent space  $\mathcal{Z}$ . The model uses a series of diffeomorphisms implemented by multilayered neural networks

$$\mathbf{x} \xleftrightarrow{f_1} \mathbf{h}_1 \xleftrightarrow{f_2} \mathbf{h}_2 \cdots \xleftrightarrow{f_n} \mathbf{z} \quad (1)$$

like flow. The whole bijective transformation  $f(\mathbf{x}) = f_n \circ f_{n-1} \cdots f_1(\mathbf{x})$  can be seen as encoder, and the inverse function  $f^{-1}(\mathbf{z})$  is used as decoder. According to the change of variable rule, the probability density function of the model can be formulated as

$$\begin{aligned} \log p_X(\mathbf{x}) &= \log p_Z(f(\mathbf{x})) + \log \left| \det \frac{\partial \mathbf{z}}{\partial \mathbf{x}^T} \right| \\ &= \log p_Z(f(\mathbf{x})) + \sum_{i=1}^n \log \left| \det \frac{\partial \mathbf{h}_i}{\partial \mathbf{h}_{i-1}^T} \right| \end{aligned} \quad (2)$$

where  $\mathbf{x} = \mathbf{h}_0, \mathbf{z} = \mathbf{h}_n, \frac{\partial \mathbf{h}_i}{\partial \mathbf{h}_{i-1}^T}$  is the Jacobian of  $f_i$ .

Here prior  $p_\theta(\mathbf{z})$  is chosen as tractable density function. For example, the most popular prior is isotropic multivariate Gaussian  $\mathcal{N}(0, I)$ , which makes  $\log p_\theta(\mathbf{z}) = -(1/2) \times \sum_i \mathbf{z}_i^2 + C$ . After training, one can sample noise  $\epsilon$  from prior and generate new samples  $f^{-1}(\epsilon)$ .

**Variational Autoencoder (VAE)** is directed graphical model approximating the data distribution  $p(\mathbf{x})$  with encoder-decoder architecture. The probabilistic encoder  $q_\phi(\mathbf{z}|\mathbf{x})$  approximates the unknown intractable posterior  $p(\mathbf{z}|\mathbf{x})$ . The probabilistic decoder  $p_\theta(\mathbf{x}|\mathbf{z})$  approximates  $p(\mathbf{x}|\mathbf{z})$ . In VAE, the variational lower bound of the marginal likelihood of data points (ELBO)

$$\begin{aligned} \mathcal{L}(\theta, \phi) &= \frac{1}{N} \sum_{i=1}^N E_{z \sim q_\phi} [\log p_\theta(\mathbf{x}^i | \mathbf{z})] - KL[q_\phi(\mathbf{z} | \mathbf{x}^i) || p(\mathbf{z})] \end{aligned} \quad (3)$$

can be optimized by stochastic gradient descent. After training, one can sample  $\mathbf{z}$  from prior  $p(\mathbf{z})$  and use the decoder  $p_\theta(\mathbf{x}|\mathbf{z})$  to generate new samples.

## 2.2 Attacking the Likelihood

We train Glow with 768-dimensional isotropic Gaussian prior on FashionMNIST. Figure 1(a) shows the histogram of log-likelihood of representations under prior ( $\log p(\mathbf{z})$ ) for different datasets. Note that  $\log p(\mathbf{z})$  of FashionMNIST are around  $-768 \times (0.5 \times \ln 2\pi e) \approx -1089.74$ , which is the log-probability of typical set of the prior [15].

Here it seems hopeful to detect OOD data by  $p(\mathbf{z})$  or typicality test in the latent space [13]. However, we scale each OOD data representation  $\mathbf{z}$  to  $\mathbf{z}' = \sqrt{d} \times \mathbf{z} / |\mathbf{z}|$ , where  $\sqrt{d}$  is the radius of the annulus of typical set, and find that  $\mathbf{z}'$  corresponds to the similar image with  $\mathbf{z}$  (details are shown in the Appendix). This demonstrates that typicality test in the latent space is not qualified for OOD detection.

Figure 1(b) shows that Glow assigns higher (lower)  $p(\mathbf{x})$  for MNIST (notMNIST). Ty-test can handle problems where the expectations of  $p(\mathbf{x})$  of inputs and training set diverge (for example, FashionMNIST vs MNIST/notMNIST) [35]. However, Ty-test fails on CIFAR10 vs CIFAR100 on Glow, because the likelihood distributions of InD and OOD datasets coincide (Figure 1(c)).

In fact, the likelihood distribution can be manipulated by adjusting the variance of inputs [34]. In Figure 2 we show the  $\log p(\mathbf{x})$  of SVHN, SVHN with increased contrast by a factor of 2.0 (SVHN-HIGH-CONTRAST) and SVHN with decreased contrast by a factor of 0.3 (SVHN-GRAY) on Glow trained on CIFAR10. The likelihood distributions of SVHN-HIGH-CONTRAST and CIFAR10 coincide. As a result, Ty-test performs worse than random guessing. Similarly, in VAE, we can also manipulate the likelihood distribution by adjusting the contrast of images. Note that, these manipulations are easy to perform because the model is treated as a black box.

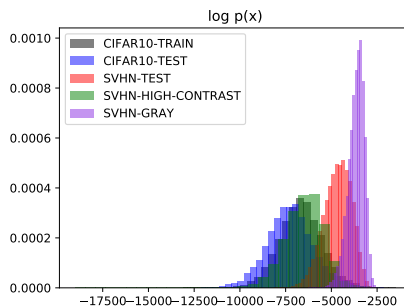


Figure 2: Glow trained on CIFAR10. Histogram of  $\log p(\mathbf{x})$ .

## 2.3 Problem

In this paper, we focus on flow-based model and VAE. We are interested in the following two questions:

1. *Why cannot we sample out new data similar to OOD data although they have higher likelihoods?*
2. *How to detect OOD data using DGM?*

Particularly, we focus on group anomaly detection [11]. Assume that we are provided a set of training data  $\{x_1, \dots, x_n\}$  drawn independently from an unknown distribution  $p^*$ , and a batch of test inputs  $\{\tilde{x}_1, \dots, \tilde{x}_m\} (m > 1)$ . Our task is to train a DGM and determine whether the test batch was drawn from  $p^*$ . This is different from pointwise anomaly detection where a single data point is provided at test time. The collective behavior of the whole test batch can be anomalous when the individual data point is seemingly regular.

### 3 Theory

In this section, we give out a theoretical explanation for why we cannot sample out new data similar to OOD dataset, although they may have higher likelihoods. Our analysis reveals that the reason is the divergence between the distribution of representations of OOD data and prior. We prove that, for a well-trained flow-based model, the distance between the distribution of representations of OOD dataset and prior can be large enough, as long as the distance between the distributions of InD and OOD dataset is large enough. In our analysis, we use  $\phi$ -divergence (also called  $f$ -divergence) defined by:

**Definition 1 ( $\phi$ -divergence)** *The  $\phi$ -divergence between two densities  $p(\mathbf{x})$  and  $q(\mathbf{x})$  is defined by*

$$D_\phi(p, q) = \int \phi\left(\frac{p(\mathbf{x})}{q(\mathbf{x})}\right)q(\mathbf{x})d\mathbf{x}, \quad (4)$$

where  $\phi$  is a convex function on  $[0, \infty)$  such that  $\phi(1) = 0$ . When  $q(\mathbf{x}) = 0$ ,  $0\phi(0/0) = 0$  and  $0\phi(p/0) = \lim_{t \rightarrow \infty} \phi(t)/t[1]$ .

$\phi$ -divergence is important to machine learning fields. Many commonly used measures including the KL divergence, Jensen-Shannon divergence, and squared Hellinger distance belong to  $\phi$ -divergence family. Many  $\phi$ -divergences are not proper distance metrics and do not satisfy the triangle inequality. We also use  $(h, \phi)$ -divergence defined by:

**Definition 2 ( $(h, \phi)$ -divergence)** *The  $(h, \phi)$ -divergence between two densities  $p(\mathbf{x})$  and  $q(\mathbf{x})$  is defined by*

$$D_\phi^h(p, q) = h(D_\phi(p, q)), \quad (5)$$

where  $h$  is a differentiable increasing real function from  $[0, \phi(0) + \lim_{t \rightarrow \infty} \phi(t)/t]$  onto  $[0, \infty)$  [32].

$(h, \phi)$ -divergence includes a broader range of divergences than  $\phi$ -divergence. For example, Rényi distance belongs to  $(h, \phi)$ -divergence family.

**Theorem 1** *Given a flow-based model  $\mathbf{z} = f(\mathbf{x})$  with prior  $p_r$ . Let  $X_1$  and  $X_2$  be two random variables and  $Z_1 = f(X_1)$ ,  $Z_2 = f(X_2)$ . Suppose that  $X_1 \sim p_X(x)$ ,  $X_2 \sim q_X(x)$ ,  $Z_1 \sim p_Z(z)$  and  $Z_2 \sim q_Z(z)$ . Let  $D$  be a proper statistical distance metric belonging to the  $(h, \phi)$ -divergence family. Then*

- (a)  $D_\phi^h(p_X, q_X) = D_\phi^h(p_Z, q_Z)$  holds.
- (b)  $D(q_Z, p_r)$  can be large enough as long as  $D(p_X, q_X)$  is large enough and  $D(p_Z, p_r)$  is small enough.

**Proof 3.1** (a) Since  $D_\phi^h(p, q) = h(D_\phi(p, q))$ , it suffices to prove  $D_\phi(p_X, q_X) = D_\phi(p_Z, q_Z)$ .

$$\begin{aligned} & D_\phi(p_Z, q_Z) \\ &= \int \phi\left(\frac{p_Z(\mathbf{z})}{q_Z(\mathbf{z})}\right)q_Z(\mathbf{z})d\mathbf{z} \\ &= \int \phi\left(\frac{p_Z(f(\mathbf{x}))}{q_Z(f(\mathbf{x}))}\right)q_Z(f(\mathbf{x}))\left|\det \frac{\partial f(\mathbf{x})}{\partial \mathbf{x}^T}\right|d\mathbf{x} \\ &= \int \phi\left(\frac{p_Z(f(\mathbf{x}))\left|\det \frac{\partial f(\mathbf{x})}{\partial \mathbf{x}^T}\right|}{q_Z(f(\mathbf{x}))\left|\det \frac{\partial f(\mathbf{x})}{\partial \mathbf{x}^T}\right|}\right)q_Z(f(\mathbf{x}))\left|\det \frac{\partial f(\mathbf{x})}{\partial \mathbf{x}^T}\right|d\mathbf{x} \\ &= \int \phi\left(\frac{p_X(\mathbf{x})}{q_X(\mathbf{x})}\right)q_X(\mathbf{x})d\mathbf{x} \\ &= D_\phi(p_X, q_X) \end{aligned} \quad (6)$$

where the first equality follows from the definition of  $\phi$ -divergence, the second equality follows from the change of variables rule in integral, the fourth equalities follows from the fact that flow-based model is diffeomorphism and  $p_X(\mathbf{x}) = p_Z(f(\mathbf{x}))\left|\det \frac{\partial f(\mathbf{x})}{\partial \mathbf{x}^T}\right|$ , which also follows from the change of variables rule.

- (b) Since  $D$  is a proper statistical distance metric and satisfies the triangle inequality, we have  $D(p_Z, p_r) + D(q_Z, p_r) \geq D(p_Z, q_Z)$ . For any  $d > 0$  and  $\epsilon > 0$ , if  $D(p_Z, q_Z) > d + \epsilon$  and  $D(p_Z, p_r) < \epsilon$ , we have  $D(q_Z, p_r) > d$ . Since  $D$  belongs to the  $(h, \phi)$ -divergence family, from Theorem (a), we know that  $D(p_X, q_X)$  equals to  $D(p_Z, q_Z)$  and can be large enough. Thus we have Theorem (b).  $\square$

Figure 3 illustrates how Theorem 1 guarantees that the distribution of OOD data representations is far enough from the prior, where InD and OOD datasets subject to  $p_X$  and  $q_X$  respectively, the representations of InD and OOD datasets subject to  $p_Z$  and  $q_Z$  respectively,  $p_r$  is the prior.

1. In practice, InD and OOD datasets are distinguishable enough for human. Take the squared Hellinger distance  $H^2(p_X, q_X) = 1 - \int \sqrt{p_X(\mathbf{x})q_X(\mathbf{x})}d\mathbf{x}$  as example. When an input  $\mathbf{x}$  belongs to only one dataset,  $p_X(\mathbf{x})q_X(\mathbf{x})$  is negligible. Therefore,  $H^2(p_X, q_X)$  is large enough, no matter what  $p_X(\mathbf{x})$  and  $q_X(\mathbf{x})$  are.

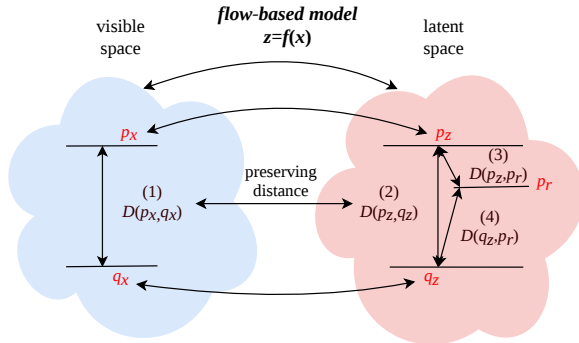


Figure 3: Overview of the proof of Theorem 1.

2. For a well-trained flow-based model, the representations of InD dataset nearly subjects to  $p_r$ . Thus,  $D(p_z, p_r)$  is small enough.
3. According to theorem 1,  $D(q_z, p_r)$  can be large enough.

Theorem 1 not only explains why we cannot sample out images similar to OOD dataset according to prior, but also prompts us that we can detect OOD data by estimating the distance between the distribution of representations and prior. In fact, *under the stronger condition  $p_z \approx p_r$ , we can have  $D_\phi^h(q_z||p_r) \approx D_\phi^h(q_z||p_z)$  directly and know that  $D_\phi^h(q_z||p_r)$  is large enough.* Therefore, in practice, we can explore any  $(h, \phi)$ -divergences rather than only the proper distance metric. In this paper, we explore the most commonly used  $(h, \phi)$ -divergence, KL divergence, for OOD detection. More divergence measures will be explored in future work.

## 4 OOD Detection Method

In this section, we discuss why and how to use KL divergence for OOD detection in DGM.

### 4.1 Investigating Representations

#### 4.1.1 Flow-based Model

In flow-based model, the representations of InD data are trained to subject to the prior. For a well-trained model, we can consider that  $p_z$  is close enough to  $p_r$ . We use the fitted Gaussian  $\mathcal{N}_Z^p$  to approximate  $p_z$  and have  $KL(p_z||p_r) \approx KL(\mathcal{N}_Z^p||p_r)$ . This is also the total correlation based on fitted Gaussian against prior [31].

On the other hand, for OOD data, the unknown  $q_z$  is far enough from  $p_r$ . It is not easy to estimate the KL divergence between unknown distributions [8]. Indeed, we need an estimation method qualified for OOD detection. Our question is can we still use fitted Gaussian when estimating  $KL(q_z||p_r)$  for OOD detection?

We train Glow on CIFAR10 and sample noises from the fitted Gaussian from representations of notMNIST<sup>1</sup>. Surprisingly, as shown in Figure 4, we can generate nearly grayscale images similar to notMNIST, although the image quality is limited. Similarly, from a single Glow model trained on CIFAR10, we can generate images with the style of multiple OOD datasets, including (not)MNIST, SVHN, CelebA, etc. (shown in the Appendix). This phenomenon can be also observed in Glow trained on other datasets. This indicates that the fitted Gaussian from representations can be treated as an important characteristic of a dataset.

We also investigate the correlation of representations. Experimental results show that, for all model-dataset pairs, the representations of OOD dataset are more correlated than that of InD dataset. For example, Figure 5 shows the histogram of non-diagonal elements of correlation of representations in Glow trained on CIFAR10 (more results are shown in the Appendix). This is not surprising because  $D_\phi^h(p_z||p_r)$  is smaller than  $D_\phi^h(q_z||p_r)$ . In fact, the high correlation of representations also explains why we cannot sample out new data similar to OOD dataset.

**Summary.** Total correlation is defined by KL divergence which belongs to  $(h, \phi)$ -divergence family. The representations of OOD data are more correlated. Thus, we propose using total correlation of representations to detect OOD data.

#### 4.1.2 VAE

It is well-known that VAE and multiple variations learn independent representations [10, 25, 12, 29, 31]. The probabilistic encoder  $q_\phi(\mathbf{z}|\mathbf{x})$  is often chosen as Gaussian form  $\mathcal{N}_Z(\boldsymbol{\mu}(\mathbf{x}), \text{diag}(\boldsymbol{\sigma}(\mathbf{x})^2))$ , where  $\mathbf{z} \sim q_\phi(\mathbf{z}|\mathbf{x})$  is used as sampled representation of  $\mathbf{x}$  and  $\boldsymbol{\mu}(\mathbf{x})$  as mean representation. The KL term in variational evidence lower bound objective can be rewritten as

$$E_{p(\mathbf{x})}[KL(q_\phi(\mathbf{z}|\mathbf{x})||p(\mathbf{z}))] = I(\mathbf{x}; \mathbf{z}) + KL(q(\mathbf{z})||p(\mathbf{z})), \quad (7)$$

<sup>1</sup>We replicate channels and pad zeros around  $28 \times 28$  notMNIST to  $32 \times 32$  for consistency.



Figure 4: Glow trained on CIFAR10. Generated images from prior (up), fitted Gaussian from representations of notMNIST (down).

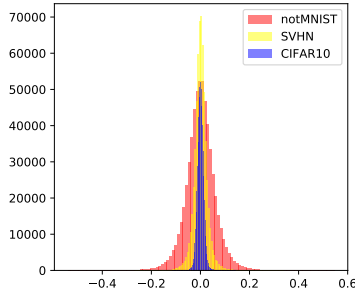


Figure 5: Glow trained on CIFAR10 and tested on notMNIST/SVHN. Histogram of non-diagonal elements of correlation of representations.

where  $p(\mathbf{z})$  is the prior,  $q(\mathbf{z})$  the aggregated posterior and  $I(\mathbf{x}; \mathbf{z})$  the mutual information between  $\mathbf{x}$  and  $\mathbf{z}$  [24]. Here  $KL(q(\mathbf{z})||p(\mathbf{z}))$  punishes the total correlation and hence encourages independent sampled representations. On the other hand, the representations of OOD dataset do not subject to prior, otherwise we can generate images similar to the OOD dataset.

The state-of-the-art  $\phi$ -divergence estimation method applicable for VAE is RAM-MC [39]. However, we find that RAM-MC can also be attacked by data manipulation (see Section 2.2). Note that, this does not prove that RAM-MC is fragile for general-purpose divergence estimation.

Similar to flow-based model, we also observed that the sampled (mean) representations of OOD datasets are more correlated in VAE. For example, we train convolutional VAE with 8-dimensional latent space on FashionMNIST. Figure 6 shows the histogram of non-diagonal elements of correlation of sampled representations (More details are shown in the Appendix). Thus, we propose using fitted Gaussian in estimating both  $KL(p_Z||p_r)$  and  $KL(q_Z||p_r)$  for OOD detection.

Note that, we use the total correlation based on fitted Gaussian against prior mostly because the representations of OOD data are more correlated. Fitted Gaussian is not always a good choice for estimating other divergence measures even under flow-based model. For example, experimental results show that the Hellinger distance between fitted Gaussian and prior is not a good criterion for OOD detection.

## 4.2 Algorithm

We propose detecting OOD dataset according to the total correlation of representations. Given a batch of inputs  $X = \{x_1, \dots, x_m\}$ , we compute the representations of  $X$  as  $Z = \{z_1, \dots, z_m\}$ . We treat  $Z$  as  $m$  observations of a  $d$ -dimensional random vector. If the total correlation is greater than a threshold  $t$ , then the input batch is determined as OOD data, otherwise, determined as InD data. In practice, we can generalize to other correlation evaluation methods. In this paper, we select the following two methods.

1. **TC**: total correlation based on a fitted Gaussian of the representations against the prior.
2.  **$\sigma$ -Corr**: the variance of the non-diagonal elements of correlation of representations.

Algorithm 1 shows the details of our method. We name our algorithm as DOCR for *Detecting OOD data by (Total) Correlation of Representations*. Particularly, we note our algorithm with the two correlation evaluation methods as DOCR-TC and DOCR- $\sigma$ -Corr respectively.

Specially, for flow-based model, the representation  $\mathbf{z} = f(\mathbf{x})$  has shape  $(H, W, C)$ , where  $H$  is the height,  $W$  the width and  $C$  the number of channels. For a batch of  $m$  inputs, the representations are treated as  $m \times H \times W$  observations of a  $C$ -dimensional random vector. We find that such modified algorithm needs a smaller batch size. In the following, we note the modified algorithm as DOCR-TC-M.

We don't use *bootstrap* [17, 3, 35] to establish the threshold. This is because bootstrap method uses sampling with replacement, and hence severely overestimates the correlation. In the experiments, we use threshold-independent metrics: area under the receiver operating characteristic curve (AUROC) and area under the precision-recall curve (AUPR) to

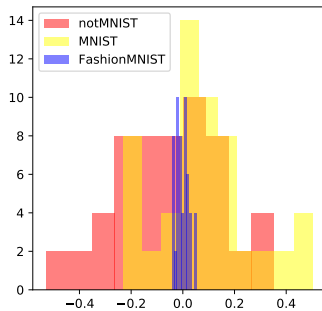


Figure 6: VAE trained on FashionMNIST and tested on MNIST/notMNIST. Histogram of non-diagonal elements of correlation of sampled representations.

---

**Algorithm 1** Out-of-Distribution data detection according to (Total) Correlation of Representations (DOCR)

---

- 1: **Input:**  $f(\mathbf{x})$ : the encoder of a well-trained flow-based model or VAE using factorized prior;  $X = \{\mathbf{x}_1, \dots, \mathbf{x}_m\}$ : a batch of inputs;  $t$ : threshold
  - 2: compute  $Z = \{z_1, \dots, z_m\}$  where  $z_i = f(\mathbf{x}_i)$
  - 3:  $c = \text{CorrelationEval}(Z)$
  - 4: **if**  $c > t$  **then**
  - 5:   return  $X$  is out-of-distribution data
  - 6: **else**
  - 7:   return  $X$  is in-distribution data
  - 8: **end if**
- 

evaluate our method.

## 5 Experiments

### 5.1 Experimental Setting

We evaluate our OOD detection algorithm with benchmarks that are used prevalently in deep anomaly detection research [34, 35, 30, 42, 20, 21], including MNIST, FashionMNIST, notMNIST, CIFAR10/100, SVHN, CelebA, and Imagenet32. We use  $S\text{-}C(k)$  ( $k \geq 0$ ) to denote dataset  $S$  with adjusted contrast by a factor  $k^2$ . For example, SVHN-C(2.0) denotes SVHN with increased contrast by a factor 2.0. Examples of these mutated datasets are shown in the Appendix. The size of each test dataset is fixed to 10,000 for comparison.

For flow-based model, we use OpenAI’s open-source implementation of Glow<sup>3</sup> with 768-dimensional isotropic Gaussian as prior except for CIFAR10 vs other problems. Specifically, for CIFAR10, we use the model checkpoint released by the authors of [35] at DeepMind for fairness<sup>4</sup>, which uses prior with learned mean and diagonal covariance. For VAE, we train convolutional VAE and use sampled representation for all problems. More details about the models are described in the Appendix.

We use threshold-independent metrics: area under the receiver operating characteristic curve (AUROC) and area under the precision-recall curve (AUPR) to evaluate our method [9]. The ROC curve shows both the true positive rate (TPR) and false positive rate (FPR) against each other when the threshold varies. An ideal detector gives 100% AUROC and a random detector gives 50% AUROC. We treat OOD data as positive data. In evaluation, each dataset is divided into batches of size  $m$ . We compute AUROC and AUPR according to the portion of batches determined as OOD data.

We use Ty-test [35] as the baseline. For comparison, we reimplement Ty-test as follows. We compute  $\hat{\epsilon}_k = |(-1/M)\sum_{m=1}^M \log p(\tilde{\mathbf{x}}_m) - \hat{\mathbb{H}}^N[p(\mathbf{x}; \theta)]|$  in the Algorithm 1 in [35], where  $\hat{\mathbb{H}}$  is the estimated entropy of the model distribution. We use  $\hat{\epsilon}_k$  as the criterion to compute AUROC and AUPR.

We find that DOCR-TC(-M) needs a smaller batch size than DOCR- $\sigma$ -Corr, except for the CIFAR10 vs CIFAR100 problem on Glow. We mainly report the results of DOCR-TC(-M) and leave most results of DOCR- $\sigma$ -Corr in the Appendix.

Due to resource limitations, we train each model once and run each method 5 times in evaluation. For each problem, we show “mean $\pm$ std” in tables.

<sup>2</sup>The contrast is adjusted channel wisely by  $x = (x - \mu) \times k + \mu$ , where  $\mu$  is the expectation of the channel,  $k$  is the factor.

<sup>3</sup><https://github.com/openai/glow>

<sup>4</sup><https://github.com/y0ast/Glow-PyTorch>. At the time of writing, this is the only model checkpoint released by the authors of [35]



## 5.2 Experimental Results

### 5.2.1 Flow-based Model

Table 1: Results on Glow trained on FashionMNIST (Fash.), SVHN, CIFAR10 and CelebA respectively We use different contrast factor to attack Ty-test. Each row is for one problem.

InD↓	OOD↓	Batch size	$m=5$		$m=10$		$m=10$		$m=25$	
		Method	DOCR-TC-M		DOCR-TC-M		Ty-test		Ty-test	
		Metric	AUROC	AUPR	AUROC	AUPR	AUROC	AUPR	AUROC	AUPR
Fash.	MNIST	<b>100.0±0.0</b>	<b>100.0±0.0</b>	<b>100.0±0.0</b>	<b>100.0±0.0</b>	99.2±0.1	98.8±0.1	<b>100.0±0.0</b>	<b>100.0±0.0</b>	
	MNIST-C(10.0)	<b>100.0±0.0</b>	<b>100.0±0.0</b>	<b>100.0±0.0</b>	<b>100.0±0.0</b>	84.9±0.3	77.6±1.3	94.7±0.3	92.4±1.0	
	notMNIST	<b>100.0±0.0</b>	<b>100.0±0.0</b>	<b>100.0±0.0</b>	<b>100.0±0.0</b>	92.7±0.5	92.0±0.6	98.9±0.2	98.8±0.3	
	notMNIST-C(0.005)	<b>100.0±0.0</b>	<b>100.0±0.0</b>	<b>100.0±0.0</b>	<b>100.0±0.0</b>	7.0±0.6	31.8±0.1	2.7±0.2	31.0±0.0	
SVHN	CelebA	<b>100.0±0.0</b>	<b>100.0±0.0</b>	<b>100.0±0.0</b>	<b>100.0±0.0</b>	<b>100.0±0.0</b>	<b>100.0±0.0</b>	<b>100.0±0.0</b>	<b>100.0±0.0</b>	
	CelebA-C(0.08)	<b>100.0±0.0</b>	<b>100.0±0.0</b>	<b>100.0±0.0</b>	<b>100.0±0.0</b>	54.7±0.5	48.8±0.3	58.2±0.3	51.1±0.3	
	CIFAR10	99.6±0.0	99.7±0.1	<b>100.0±0.0</b>	<b>100.0±0.0</b>	<b>100.0±0.0</b>	<b>100.0±0.0</b>	<b>100.0±0.0</b>	<b>100.0±0.0</b>	
	CIFAR10-C(0.12)	99.1±0.0	99.2±0.0	<b>100.0±0.0</b>	<b>100.0±0.0</b>	54.7±0.5	48.8±0.3	12.6±0.9	32.6±0.2	
	CIFAR100	99.6±0.0	99.7±0.0	<b>100.0±0.0</b>	<b>100.0±0.0</b>	<b>100.0±0.0</b>	<b>100.0±0.0</b>	<b>100.0±0.0</b>	<b>100.0±0.0</b>	
	CIFAR100-C(0.12)	99.0±0.1	100.0±0.0	<b>100.0±0.0</b>	<b>100.0±0.0</b>	26.9±1.3	36.2±0.4	12.0±1.1	32.4±0.2	
	Imagenet32	<b>100.0±0.0</b>	<b>100.0±0.0</b>	<b>100.0±0.0</b>	<b>100.0±0.0</b>	<b>100.0±0.0</b>	<b>100.0±0.0</b>	<b>100.0±0.0</b>	<b>100.0±0.0</b>	
	Imagenet32-C(0.07)	<b>100.0±0.0</b>	<b>100.0±0.0</b>	<b>100.0±0.0</b>	<b>100.0±0.0</b>	42.6±0.4	44.1±0.2	35.7±0.3	40.8±0.2	
CIFAR10	CelebA	<b>100.0±0.0</b>	<b>100.0±0.0</b>	<b>100.0±0.0</b>	<b>100.0±0.0</b>	<b>100.0±0.0</b>	<b>100.0±0.0</b>	<b>100.0±0.0</b>	<b>100.0±0.0</b>	
	CelebA-C(0.3)	98.4±0.0	98.5±0.0	<b>100.0±0.0</b>	<b>100.0±0.0</b>	23.4±5.3	35.1±0.2	12.6±0.7	32.6±0.1	
	Imagenet32	97.5±0.2	97.8±0.1	<b>100.0±0.0</b>	<b>100.0±0.0</b>	<b>100.0±0.0</b>	<b>100.0±0.0</b>	<b>100.0±0.0</b>	<b>100.0±0.0</b>	
	Imagenet32-C(0.3)	89.8±0.6	90.2±0.6	<b>99.5±0.0</b>	<b>99.5±0.0</b>	31.7±0.7	38.3±0.2	15.0±1.0	33.0±0.2	
	SVHN	<b>100.0±0.0</b>	<b>100.0±0.0</b>	<b>100.0±0.0</b>	<b>100.0±0.0</b>	<b>100.0±0.0</b>	<b>100.0±0.0</b>	<b>100.0±0.0</b>	<b>100.0±0.0</b>	
	SVHN-C(2.0)	<b>100.0±0.0</b>	<b>100.0±0.0</b>	<b>100.0±0.0</b>	<b>100.0±0.0</b>	26.7±0.5	58.0±0.1	15.1±54.1	0.9±0.3	
CelebA	CIFAR10	91.4±0.4	91.7±0.3	<b>99.2±0.0</b>	<b>99.2±0.0</b>	1.0±0.1	30.8±0.0	0.0±0.0	30.7±0.0	
	CIFAR100	93.6±0.3	94.0±0.2	<b>99.5±0.0</b>	<b>99.5±0.0</b>	2.0±0.2	30.8±0.0	0.0±0.0	30.7±0.0	
	Imagenet32	99.9±0.0	99.9±0.0	<b>100.0±0.0</b>	<b>100.0±0.0</b>	87.9±0.3	90.5±0.1	96.7±0.4	97.4±0.2	
	Imagenet32-C(0.07)	99.9±0.0	99.9±0.0	<b>100.0±0.0</b>	<b>100.0±0.0</b>	23.0±0.3	36.4±0.2	11.7±0.3	32.4±0.2	
	SVHN	<b>100.0±0.0</b>	<b>100.0±0.0</b>	<b>100.0±0.0</b>	<b>100.0±0.0</b>	91.5±0.6	89.9±1.4	98.6±0.2	98.5±0.2	
	SVHN-C(1.8)	<b>100.0±0.0</b>	<b>100.0±0.0</b>	<b>100.0±0.0</b>	<b>100.0±0.0</b>	1.4±0.2	30.8±0.0	0.0±0.0	30.7±0.0	

**Unconditional Glow.** Table 6 shows the results on Glow trained on FashionMNIST, SVHN, CIFAR10, CelebA and tested on other datasets as OOD data. We can see that for all these problems, DOCR-TC-M can achieve (nearly) 100% AUROC/AUPR with batch size 10 and outperforms Ty-test significantly. Importantly, for different problems, we adjust the contrast with different factors such that InD and OOD data have coinciding likelihood distributions, and hence Ty-test fails. On the contrary, our method is robust against data manipulation. We find that DOCR-TC needs a larger batch size than DOCR-TC-M, but still outperforms Ty-test. More results of DOCR-TC are shown in the Appendix.

Table 2 shows the results on CIFAR10 vs CIFAR100 problem, which is not solved by Ty-test. This is also the hardest problem for our method. DOCR- $\sigma$ -Corr achieves 92%+AUROC when the batch size reaches 250 while DOCR-TC(-M) fails. We consider the main reason is that the model fails to capture the distribution of CIFAR10 as successfully as in other problems (see Figure 4). Thus,  $D(p_Z, p_r)$  is not small enough. So Theorem 1 does not fit well for this problem. Results with model checkpoints released by OpenAI<sup>5</sup> is shown in the Appendix.

CelebA vs CIFAR10/100 is also challenging for Ty-test [35], while our method can achieve 100% AUROC. We should point out that, the experimental results on Glow trained on CelebA is not fair for Ty-test, because we were not able to make the likelihood distribution of CelebA training split and test split fit well<sup>6</sup>. The likelihood distributions of CIFAR10/CIFAR100 test split and CelebA training split are closer. This misleads Ty-test to make the wrong determination. On the contrary, our method is not affected by possible underfitting or overfitting.

Table 2: Glow trained on CIFAR10 and tested on CIFAR100. Each row is for one batch size.

Method	DOCR- $\sigma$ -Corr		Ty-test	
	AUROC	AUPR	AUROC	AUPR
$m=50$	<b>69.2±0.9</b>	<b>68.7±2.7</b>	61.0±0.4	63.7±1.3
$m=100$	<b>78.9±3.6</b>	<b>78.7±3.7</b>	65.7±1.5	67.1±1.7
$m=150$	<b>86.0±1.6</b>	<b>85.4±1.0</b>	70.2±2.4	70.2±2.7
$m=200$	<b>88.0±3.1</b>	<b>88.8±1.8</b>	73.0±1.6	70.6±2.7
$m=250$	<b>92.7±2.5</b>	<b>92.6±2.5</b>	74.6±0.7	74.7±1.7

**Class conditional Glow.** We train class conditional Glow on FashionMNIST and treat each class as InD data and the rest classes as OOD data. As shown in Table 3, DOCR-TC-M can achieve nearly 100% AUROC for all cases when

<sup>5</sup><https://storage.googleapis.com/glow-demo/logs/abl-1x1-aff.tar>

<sup>6</sup>We did not search more hyperparameters due to resource limitations.



batch size is 25, while Ty-test is worse than random guessing in most cases. The reason is that the centroids of Gaussian components are close to each other. This makes OOD detection based on  $p(\mathbf{x})$  infeasible. In the Appendix, we also list the results of using  $p(\mathbf{z})$  as the criterion for pointwise anomaly detection. These results demonstrate that the likelihood of class conditional Glow is not a reliable criterion.

Table 3: Class conditional Glow trained on FashionMNIST. Treat each class as InD data and the rest classes as OOD data.

Batch size	$m=25$			
	DOCR-TC-M		Ty-test	
Method	AUROC	AUPR	AUROC	AUPR
class 0 vs rest	<b>100.0±0.0</b>	<b>100.0±0.0</b>	5.4±1.6	31.2±0.3
class 1 vs rest	<b>100.0±0.0</b>	<b>100.0±0.0</b>	15.7±2.4	33.4±4.9
class 2 vs rest	<b>100.0±0.0</b>	<b>100.0±0.0</b>	0.5±0.5	30.7±0.0
class 3 vs rest	<b>99.9±0.1</b>	<b>99.9±0.1</b>	89.6±2.5	91.3±2.3
class 4 vs rest	<b>100.0±0.0</b>	<b>100.0±0.0</b>	0.7±0.6	30.7±0.0
class 5 vs rest	<b>100.0±0.0</b>	<b>100.0±0.0</b>	64.2±1.4	66.4±2.9
class 6 vs rest	<b>99.9±0.1</b>	<b>99.9±0.1</b>	0.0±0.0	30.7±0.0
class 7 vs rest	<b>100.0±0.0</b>	<b>100.0±0.0</b>	31.4±2.8	46.6±3.3
class 8 vs rest	<b>100.0±0.0</b>	<b>100.0±0.0</b>	0.4±0.5	30.7±0.0
class 9 vs rest	<b>100.0±0.0</b>	<b>100.0±0.0</b>	69.0±3.6	76.0±1.7

## 5.2.2 VAE

We train convolutional VAE with 8-, 16- 32-dimensional latent space on FashionMNIST, SVHN, and CIFAR10 respectively. Table 4 shows the results. Generally, our method needs a larger batch size than Ty-test and robust against data manipulations. Ty-test needs a smaller batch size but can be fooled by data manipulations for almost all problems. We failed to attack Ty-test by grayed notMNIST, because even a zero contrast factor still results in lower likelihood than FashionMNIST. Again, CIFAR10 vs CIFAR100 is also the most difficult problem for our method on VAE. As shown in Table 5, DOCR-TC needs a batch size 150 to achieve 98%+ AUROC. Nevertheless, DOCR-TC still outperforms Ty-test.

Table 4: VAE trained on FashionMNIST (Fash.), SVHN and CIFAR10.

InD↓	OOD↓	Batch size	$m=10$				$m=25$			
			DOCR-TC		Ty-test		DOCR-TC		Ty-test	
			AUROC	AUPR	AUROC	AUPR	AUROC	AUPR	AUROC	AUPR
Fash.	MNIST		99.7±0.1	99.5±0.2	<b>100.0±0.0</b>	<b>100.0±0.0</b>	<b>100.0±0.0</b>	<b>100.0±0.0</b>	<b>100.0±0.0</b>	<b>100.0±0.0</b>
	MNIST-C(0.4)		<b>99.8±0.0</b>	<b>99.8±0.0</b>	39.1±0.7	40.5±0.3	<b>100.0±0.0</b>	<b>100.0±0.0</b>	37.6±1.9	39.8±0.7
	notMNIST		<b>100.0±0.0</b>	<b>100.0±0.0</b>	<b>100.0±0.0</b>	<b>100.0±0.0</b>	<b>100.0±0.0</b>	<b>100.0±0.0</b>	<b>100.0±0.0</b>	<b>100.0±0.0</b>
SVHN	CelebA		92.2±0.6	82.3±1.1	<b>100.0±0.0</b>	<b>100.0±0.0</b>	<b>100.0±0.0</b>	<b>100.0±0.0</b>	<b>100.0±0.0</b>	<b>100.0±0.0</b>
	CelebA-C(0.7)		<b>86.2±0.9</b>	<b>76.5±1.5</b>	39.9±1.2	41.2±0.5	<b>100.0±0.0</b>	<b>100.0±0.0</b>	47.4±1.5	44.3±0.7
	CIFAR10		90.9±1.3	81.3±2.3	<b>100.0±0.0</b>	<b>100.0±0.0</b>	<b>100.0±0.0</b>	<b>100.0±0.0</b>	<b>100.0±0.0</b>	<b>100.0±0.0</b>
	CIFAR10-C(0.4)		<b>77.6±8.8</b>	<b>69.9±1.3</b>	49.8±0.6	45.8±0.3	<b>99.7±0.2</b>	<b>99.6±0.3</b>	58.8±0.9	50.2±0.4
	CIFAR100		90.4±0.4	80.3±0.6	<b>100.0±0.0</b>	<b>100.0±0.0</b>	<b>100.0±0.0</b>	<b>100.0±0.0</b>	<b>100.0±0.0</b>	<b>100.0±0.0</b>
	CIFAR100-C(0.4)		<b>80.5±1.0</b>	<b>73.2±1.8</b>	40.3±0.8	40.7±1.3	<b>99.8±0.0</b>	<b>99.8±0.0</b>	40.5±0.4	41.3±0.2
	Imagenet32		89.3±8.6	80.1±1.5	<b>100.0±0.0</b>	<b>100.0±0.0</b>	<b>100.0±0.0</b>	<b>100.0±0.0</b>	<b>100.0±0.0</b>	<b>100.0±0.0</b>
	Imagenet32-C(0.3)		<b>74.6±0.6</b>	<b>67.8±0.7</b>	27.9±1.0	36.5±0.3	<b>99.0±0.0</b>	<b>99.0±0.0</b>	27.9±1.0	36.5±0.3
InD↓	OOD↓	Batch size	$m=25$				$m=50$			
CIFAR10	CelebA		99.1±0.4	99.1±0.4	<b>100.0±0.0</b>	<b>100.0±0.0</b>	<b>100.0±0.0</b>	<b>100.0±0.0</b>	<b>100.0±0.0</b>	<b>100.0±0.0</b>
	CelebA-C(0.7)		<b>94.2±0.6</b>	<b>93.8±0.8</b>	42.3±1.1	42.8±0.6	<b>100.0±0.0</b>	<b>100.0±0.0</b>	39.3±2.0	41.1±1.0
	Imagenet32		54.0±1.9	53.4±0.7	<b>99.8±0.1</b>	<b>99.8±0.1</b>	94.0±0.6	94.0±0.5	<b>100.0±0.0</b>	<b>100.0±0.0</b>
	Imagenet32-C(0.8)		<b>77.4±1.4</b>	<b>77.3±1.8</b>	47.8±1.5	48.0±1.5	<b>98.8±0.5</b>	<b>98.9±0.4</b>	46.4±1.7	46.8±1.2
	SVHN		91.8±1.5	91.1±2.3	<b>99.8±0.0</b>	<b>99.8±0.0</b>	<b>100.0±0.0</b>	<b>100.0±0.0</b>	<b>100.0±0.0</b>	<b>100.0±0.0</b>
	SVHN-C(1.5)		<b>94.2±1.5</b>	<b>91.1±2.3</b>	60.0±1.7	61.4±1.7	<b>100.0±0.0</b>	<b>100.0±0.0</b>	53.6±2.7	55.7±1.6

In the Appendix, we also list the results of using reconstruction probability for OOD data detection[2]. These results indicate that reconstruction probability is not a reliable criterion for OOD detection.

It is notable that our method is affected by the model architecture and training method in VAE. Both of high dimensional latent space and dropout used in training lead to nearly dead neurons in latent space. Dimensions with small variance can lead to strong correlation and hence reduce the performance of our method. Additionally, We did not conduct experiments on other VAE variations, which have more independent representations than vanilla VAE [31].

## 6 Related Work

**OOD detection.** Generally, it is straightforward to use a generative model model  $p(\mathbf{x})$  to detect OOD data [38]. One can select a threshold  $t$  such that the input  $\mathbf{x}$  is determined as anomaly if  $p(\mathbf{x}) < t$ . This method is used in multiple

Table 5: VAE trained on CIFAR10 and tested on CIFAR100. Each row is for one batch size.

Problem	CIFAR10 vs CIFAR100				CIFAR10 vs Imagenet32			
	DOCR-TC		Ty-test		DOCR-TC		Ty-test	
Metric	AUROC	AUPR	AUROC	AUPR	AUROC	AUPR	AUROC	AUPR
$m=50$	72.9±0.7	73.7±2.1	<b>73.8±0.5</b>	<b>74.3±1.8</b>	94.0±0.6	94.0±0.5	<b>100.0±0.0</b>	<b>100.0±0.0</b>
$m=100$	<b>90.9±1.0</b>	<b>91.3±1.3</b>	82.6±0.5	83.5±1.1	99.9±0.2	99.9±0.2	<b>100.0±0.0</b>	<b>100.0±0.0</b>
$m=150$	<b>98.0±0.4</b>	<b>98.1±0.5</b>	88.4±1.3	88.6±2.3	<b>100.0±0.0</b>	<b>100.0±0.0</b>	<b>100.0±0.0</b>	<b>100.0±0.0</b>

works [44, 6, 5, 37]. Some sophisticated method uses extreme value theory for anomaly detection[14]. However, all these methods fail when OOD data has a higher likelihood.

Recently, Choi et al. propose using the Watanabe-Akaike Information Criterion (WAIC) to detect OOD data [13]. WAIC penalizes points which are sensitive to the particular choice of posterior model parameters, and hence needs multiple models. Recently, [35] points out that WAIC is not stable.

In [13], Choi et al. also proposes using typicality test in the latent space to detect OOD data. Our results reported in section 2 demonstrate that typicality test in the latent space is inadvisable. Sabeti et al. propose detecting anomaly based on typicality [40], but their method is not suitable for DGM. Nalisnick et al. propose using typicality test on model distribution to detect OOD data [35]. Their method can be applied for flow-based model, VAE, and PixelCNN. Before this writing, [35] is the state-of-the-art method for OOD detection in DGM. However, when the likelihood of OOD data and InD data coincides, all likelihood- (typicality-) based methods would fail. Nalisnick et al. also point out that the likelihood distribution of DGM has a fundamental limitation [35]. In the experiments, we show that the likelihood of OOD data can be manipulated such that OOD and InD data have coinciding likelihood distribution. Our method is not based on likelihood and can handle all the problems we have encountered. However, our method is not applicable for auto-regressive models.

**Independent representations.** Our OOD detection method is applicable to DGM with independent representations. Theoretically, restricting to factorized prior does not hamper the expressiveness of flow-based model. Many VAE variations including  $\beta$ -VAE [23], FactorVAE [25], DIP-VAE [28] etc. have more independent sampled representations than vanilla VAE. In principle, our method is also applicable to models concerning disentangled representation learning [4]. This is because independence is a necessary condition for disentanglement although there exists no common definition of disentanglement [4, 31, 23, 47].

**Divergence estimation.** Many  $\phi$ -divergence estimation methods have been proposed [39, 8, 22]. We should select the appropriate divergences and estimation methods for OOD detection. As discussed in Section 4.1, the state-of-the-art  $\phi$ -divergence estimation method suitable for VAE can be attacked by data manipulation. Hellinger distance between fitted Gaussian and prior is not qualified either. In this paper, we use the KL divergence of fitted Gaussian from prior for OOD detection. In the future, we will explore more divergence estimation methods.

## 7 Conclusion

In this paper, we prove that, for a well-trained flow-based model, the distance between the distribution of representations of an OOD dataset and prior can be large enough, as long as the distance between the distributions of InD and OOD datasets is large enough. We also have observed that, in flow-based model and VAE with factorized prior, the representations of OOD datasets are more correlated than that of InD dataset. Based on our theorem and observation, we propose detecting OOD data by the total correlation of representations. Experimental results demonstrate that our method can achieve nearly 100% AUROC for all problems and robust against data manipulation. While the state-of-the-art method performs not better than random guessing for challenging problems and can be fooled by data manipulation in almost all cases.

## References

- [1] Syed Mumtaz Ali and Samuel D Silvey. A general class of coefficients of divergence of one distribution from another. *Journal of the Royal Statistical Society: Series B (Methodological)*, 28(1):131–142, 1966.
- [2] Jinwon An and Sungzoon Cho. Variational autoencoder based anomaly detection using reconstruction probability. *Special Lecture on IE*, 2(1), 2015.
- [3] Miguel Arcones and Evarist Gine. On the bootstrap of u and v statistics. *The Annals of Statistics*, pages 655–674, 1992.
- [4] Yoshua Bengio, Aaron Courville, and Pascal Vincent. Representation learning: A review and new perspectives. *IEEE transactions on pattern analysis and machine intelligence*, 35(8):1798–1828, 2013.

- [5] C. M. Bishop. Novelty detection and neural network validation. *IEE Proceedings - Vision, Image and Signal Processing*, 141(4):217–222, 1994.
- [6] Ronald Bremer. Outliers in statistical data, 1995.
- [7] Andrew Brock, Jeff Donahue, and Karen Simonyan. Large scale GAN training for high fidelity natural image synthesis. In *International Conference on Learning Representations*, 2019.
- [8] Yuheng Bu, Shaofeng Zou, Yingbin Liang, and Venugopal V. Veeravalli. Estimation of kl divergence: Optimal minimax rate. *IEEE Transactions on Information Theory*, pages 1–1.
- [9] Michael Buckland and Fredric Gey. The relationship between recall and precision. *Journal of the American society for information science*, 45(1):12–19, 1994.
- [10] Christopher P. Burgess, Irina Higgins, Arka Pal, Loic Matthey, Nick Watters, Guillaume Desjardins, and Alexander Lerchner. Understanding disentangling in  $\beta$ -vae. In *Workshop on Learning Disentangled Representations at the 31st Conference on Neural Information Processing Systems*, 2018.
- [11] Raghavendra Chalapathy, Edward Toth, and Sanjay Chawla. Group anomaly detection using deep generative models. In *Joint European Conference on Machine Learning and Knowledge Discovery in Databases*, pages 173–189. Springer, 2018.
- [12] Tian Qi Chen, Xuechen Li, Roger B Grosse, and David K Duvenaud. Isolating sources of disentanglement in variational autoencoders. In S. Bengio, H. Wallach, H. Larochelle, K. Grauman, N. Cesa-Bianchi, and R. Garnett, editors, *Advances in Neural Information Processing Systems 31*, pages 2610–2620. Curran Associates, Inc., 2018.
- [13] Hyunsun Choi and Eric Jang. WAIC, but why?: Generative ensembles for robust anomaly detection. *arXiv preprint arXiv:1810.01392*, 2018.
- [14] David A. Clifton, Lei Clifton, Samuel Hugueny, and Lionel Tarassenko. Extending the generalised pareto distribution for novelty detection in high-dimensional spaces. *Journal of Signal Processing Systems*, 74(3):323–339, Mar 2014.
- [15] Thomas M Cover and Joy A Thomas. *Elements of information theory*. John Wiley & Sons, 2012.
- [16] Laurent Dinh, Jascha Sohl-Dickstein, and Samy Bengio. Density estimation using real nvp. In *Proceedings of the International Conference on Learning Representations (ICLR)*, 2017.
- [17] Bradley Efron. Bootstrap methods: Another look at the jackknife. *Annals of Statistics*, 7(1):1–26, 1979.
- [18] Ethan Fetaya, Jörn-Henrik Jacobsen, and Richard S. Zemel. Conditional generative models are not robust. *CoRR*, abs/1906.01171, 2019.
- [19] Ian Goodfellow, Jean Pouget-Abadie, Mehdi Mirza, Bing Xu, David Warde-Farley, Sherjil Ozair, Aaron Courville, and Yoshua Bengio. Generative adversarial nets. In *Advances in neural information processing systems*, pages 2672–2680, 2014.
- [20] Dan Hendrycks and Kevin Gimpel. A baseline for detecting misclassified and out-of-distribution examples in neural networks. In *Proceedings of the International Conference on Learning Representations (ICLR)*, 2017.
- [21] Dan Hendrycks, Mantas Mazeika, and Thomas G Dietterich. Deep anomaly detection with outlier exposure. *International Conference on Learning Representations (ICLR)*, 2019.
- [22] Alfred O Hero, Bing Ma, Olivier Michel, and John Gorman. Alpha-divergence for classification, indexing and retrieval. *Communication and Signal Processing Laboratory, Technical Report CSPL-328, U. Mich*, 2001.
- [23] Irina Higgins, Loic Matthey, Arka Pal, Christopher Burgess, Xavier Glorot, Matthew Botvinick, Shakir Mohamed, and Alexander Lerchner. beta-vae: Learning basic visual concepts with a constrained variational framework. *ICLR*, 2(5):6, 2017.
- [24] Matthew D Hoffman and Matthew J Johnson. Elbo surgery: yet another way to carve up the variational evidence lower bound. In *Workshop in Advances in Approximate Bayesian Inference, NIPS*, volume 1, 2016.
- [25] Hyunjik Kim and Andriy Mnih. Disentangling by factorising. In Jennifer Dy and Andreas Krause, editors, *Proceedings of the 35th International Conference on Machine Learning*, volume 80 of *Proceedings of Machine Learning Research*, pages 2649–2658, Stockholmssan, Stockholm Sweden, 10–15 Jul 2018. PMLR.
- [26] Diederik P Kingma and Max Welling. Auto-encoding variational bayes. In *Proceedings of the International Conference on Learning Representations (ICLR)*, 2014.

- [27] Durk P Kingma and Prafulla Dhariwal. Glow: Generative flow with invertible 1x1 convolutions. In *Advances in Neural Information Processing Systems*, pages 10215–10224, 2018.
- [28] Abhishek Kumar, Prasanna Sattigeri, and Avinash Balakrishnan. Variational inference of disentangled latent concepts from unlabeled observations. *ICLR*, 2017.
- [29] Abhishek Kumar, Prasanna Sattigeri, and Avinash Balakrishnan. Variational inference of disentangled latent concepts from unlabeled observations. In *International Conference on Learning Representations*, 2018.
- [30] Kimin Lee, Kibok Lee, Honglak Lee, and Jinwoo Shin. A simple unified framework for detecting out-of-distribution samples and adversarial attacks. In *Advances in Neural Information Processing Systems*, pages 7167–7177, 2018.
- [31] Francesco Locatello, Stefan Bauer, Mario Lucic, Gunnar Rätsch, Sylvain Gelly, Bernhard Schölkopf, and Olivier Bachem. Challenging common assumptions in the unsupervised learning of disentangled representations. In *Proceedings of the 36th International Conference on Machine Learning*, 2019.
- [32] M. L. Menéndez, D. Morales, L. Pardo, and M. Salicrú. Asymptotic behaviour and statistical applications of divergence measures in multinomial populations: a unified study. *Statistical Papers*, 36(1):1–29, 1995.
- [33] Yishu Miao. *Deep generative models for natural language processing*. PhD thesis, University of Oxford, 2017.
- [34] Eric Nalisnick, Akihiro Matsukawa, Yee Whye Teh, Dilan Gorur, and Balaji Lakshminarayanan. Do deep generative models know what they don’t know? *International Conference on Learning Representations (ICLR)*, 2019.
- [35] Eric Nalisnick, Akihiro Matsukawa, Yee Whye Teh, and Balaji Lakshminarayanan. Detecting out-of-distribution inputs to deep generative models using typicality. *4th workshop on Bayesian Deep Learning (NeurIPS 2019)*, 2019.
- [36] Aaron van den Oord, Sander Dieleman, Heiga Zen, Karen Simonyan, Oriol Vinyals, Alex Graves, Nal Kalchbrenner, Andrew Senior, and Koray Kavukcuoglu. Wavenet: A generative model for raw audio. *arXiv preprint arXiv:1609.03499*, 2016.
- [37] Lucas C Parra, Gustavo Deco, and Stefan Miesbach. Statistical independence and novelty detection with information preserving nonlinear maps. *Neural Computation*, 8(2):260–269, 1996.
- [38] Marco A. F. Pimentel, David A. Clifton, Clifton Lei, and Lionel Tarassenko. A review of novelty detection. *Signal Processing*, 99(6):215–249, 2014.
- [39] Paul K. Rubenstein, Olivier Bousquet, Josip Djolonga, Carlos Riquelme, and Ilya O. Tolstikhin. Practical and consistent estimation of f-divergences. *Annual Conference on Neural Information Processing Systems*, abs/1905.11112:4072–4082, 2019.
- [40] Elyas Sabeti and A Hostmadsen. Data discovery and anomaly detection using atypicality for real-valued data. *Entropy*, 21(3):219, 2019.
- [41] Tim Salimans, Andrej Karpathy, Xi Chen, and Diederik P Kingma. PixelCNN++: Improving the pixelcnn with discretized logistic mixture likelihood and other modifications. *Proceedings of the International Conference on Learning Representations (ICLR)*, 2017.
- [42] Alireza Shafaei, Mark Schmidt, and James J Little. Does your model know the digit 6 is not a cat? a less biased evaluation of “outlier” detectors. *arXiv preprint arXiv:1809.04729*, 2018.
- [43] Vít Škvára, Tomáš Pevný, and Václav Šmídl. Are generative deep models for novelty detection truly better? *KDD Workshop on Outlier Detection De-Constructed (ODD v5.0)*, 2018.
- [44] Lionel Tarassenko, Paul Hayton, Nicholas Cerneaz, and Michael Brady. Novelty detection for the identification of masses in mammograms. 1995.
- [45] Aaron Van den Oord, Nal Kalchbrenner, Lasse Espeholt, Oriol Vinyals, Alex Graves, et al. Conditional image generation with pixelcnn decoders. In *Advances in neural information processing systems*, pages 4790–4798, 2016.
- [46] Roman Vershynin. *High-dimensional probability: An introduction with applications in data science*, volume 47. Cambridge University Press, 2018.
- [47] Xiaojiang Yang, Wendong Bi, Yu Cheng, and Junchi Yan. Bridging disentanglement with independence and conditional independence via mutual information for representation learning, 2019.

## A Model Details

We use both DeepMind and OpenAI’s official implementations of Glow model. The model consists of three stages, each of which contains 32 coupling layers with width 512. After each stage, the latent variables are splitted into two parts, one half is treated as the final representations and another half is processed by the next stage. We use additive coupling layers for grayscale datasets and CelebA and use affine coupling layers for SVHN and CIFAR10. All priors and standard Gaussian except for CIFAR10, which use prior with learned mean and diagonal covariance. All models are trained using Adamax optimization method with a batch size of 64. The learning rate is increased from 0 up to 0.001 in the first 10 epoches and keeps invariable in remaining epoches. Flow-based models are very resource consuming. For the sake of resource limitation, we use the checkpoints released by DeepMind<sup>7</sup> and OpenAI<sup>8</sup> for CIFAR10.

For VAE, we use convolutional architecture in the encoder and decoder. The encoder consists three  $4 \times 4 \times 64$  convolution layers. On top of convolutional layers, one dense layer produces the mean  $\mu(\mathbf{x})$  and another dense layer head of the same size produces standard variance  $\sigma(\mathbf{x})$ . The decoder has the mirrored architecture as encoder. All activations are LeakyReLU with  $\alpha = 0.3$ . For FashionMNIST, SVHN and CIFAR10, we use 8-, 16- and 32-dimensional latent space respectively. Models are trained using Adam without dropout. The learning rate is  $5 \times 10^{-4}$  with no decay. For FashionMNIST, the total epoch number is 40K, while for SVHN and CIFAR10 the total epoch numbers are 50K.

## B More Experimental Results

Table 6 shows the results of DOCR-TC on CIFAR10 vs others problems using the model checkpoint released by DeepMind. Compared to DOCR-TC-M, DOCR-TC needs a slightly larger batch size, but still outperforms Ty-test significantly.

Table 6: Results of DOCR-TC on Glow trained on FashionMNIST (Fash.M), SVHN, CIFAR10 and CelebA respectively. We use different contrast factor to attack Ty-test. Each row is for one problem. DOCR-TC needs a larger batch size than DOCR-TC-M, but still outperforms Ty-test significantly.

InD↓	OOD↓	Batch size	$m=10$				$m=25$			
		Method	DOCR-TC		Ty-test		DOCR-TC		Ty-test	
		Metric	AUROC	AUPR	AUROC	AUPR	AUROC	AUPR	AUROC	AUPR
Fash.M	MNIST		<b>100.0±0.0</b>	<b>100.0±0.0</b>	99.2±0.1	98.8±0.1	<b>100.0±0.0</b>	<b>100.0±0.0</b>	<b>100.0±0.0</b>	<b>100.0±0.0</b>
	MNIST-C(10.0)		<b>100.0±0.0</b>	<b>100.0±0.0</b>	84.9±0.3	77.6±1.3	<b>100.0±0.0</b>	<b>100.0±0.0</b>	94.7±0.3	92.4±1.0
	notMNIST		<b>100.0±0.0</b>	<b>100.0±0.0</b>	92.7±0.5	92.0±0.6	<b>100.0±0.0</b>	<b>100.0±0.0</b>	98.9±0.2	98.8±0.3
	notMNIST-C(0.005)		<b>100.0±0.0</b>	<b>100.0±0.0</b>	7.0±0.6	31.8±0.1	<b>100.0±0.0</b>	<b>100.0±0.0</b>	2.7±0.2	31.0±0.0
SVHN	CelebA		<b>100.0±0.0</b>	<b>100.0±0.0</b>	<b>100.0±0.0</b>	<b>100.0±0.0</b>	<b>100.0±0.0</b>	<b>100.0±0.0</b>	<b>100.0±0.0</b>	<b>100.0±0.0</b>
	CelebA-C(0.08)		<b>100.0±0.0</b>	<b>100.0±0.0</b>	54.7±0.5	48.8±0.3	<b>100.0±0.0</b>	<b>100.0±0.0</b>	58.2±0.3	51.1±0.3
	CIFAR10		<b>100.0±0.0</b>	<b>100.0±0.0</b>	<b>100.0±0.0</b>	<b>100.0±0.0</b>	<b>100.0±0.0</b>	<b>100.0±0.0</b>	<b>100.0±0.0</b>	<b>100.0±0.0</b>
	CIFAR10-C(0.12)		<b>100.0±0.0</b>	<b>100.0±0.0</b>	54.7±0.5	48.8±0.3	<b>99.1±0.3</b>	<b>99.4±0.4</b>	12.6±0.9	32.6±0.2
	CIFAR100		<b>100.0±0.0</b>	<b>100.0±0.0</b>	<b>100.0±0.0</b>	<b>100.0±0.0</b>	<b>100.0±0.0</b>	<b>100.0±0.0</b>	<b>100.0±0.0</b>	<b>100.0±0.0</b>
	CIFAR100-C(0.12)		<b>95.5±0.4</b>	<b>95.8±0.5</b>	26.9±1.3	36.2±0.4	<b>97.2±0.2</b>	<b>97.6±0.0</b>	12.0±1.1	32.4±0.2
	Imagenet32		<b>100.0±0.0</b>	<b>100.0±0.0</b>	<b>100.0±0.0</b>	<b>100.0±0.0</b>	<b>100.0±0.0</b>	<b>100.0±0.0</b>	<b>100.0±0.0</b>	<b>100.0±0.0</b>
	Imagenet32-C(0.07)		<b>100.0±0.0</b>	<b>100.0±0.0</b>	42.6±0.4	44.1±0.2	<b>100.0±0.0</b>	<b>100.0±0.0</b>	35.7±0.3	40.8±0.2
CIFAR10	CelebA		<b>100.0±0.0</b>	<b>100.0±0.0</b>	<b>100.0±0.0</b>	<b>100.0±0.0</b>	<b>100.0±0.0</b>	<b>100.0±0.0</b>	<b>100.0±0.0</b>	<b>100.0±0.0</b>
	CelebA-C(0.3)		<b>100.0±0.0</b>	<b>100.0±0.0</b>	23.4±5.3	35.1±0.2	<b>100.0±0.0</b>	<b>100.0±0.0</b>	12.6±0.7	32.6±0.1
	Imagenet32		99.3±0.0	99.4±0.0	<b>100.0±0.0</b>	<b>100.0±0.0</b>	99.0±0.3	99.2±0.2	<b>100.0±0.0</b>	<b>100.0±0.0</b>
	Imagenet32-C(0.3)		<b>94.8±0.3</b>	<b>95.2±0.3</b>	31.7±0.7	38.3±0.2	<b>96.7±0.5</b>	<b>97.4±0.4</b>	15.0±1.0	33.0±0.2
	SVHN		99.1±0.0	99.7±0.0	<b>99.9±0.0</b>	<b>100.0±0.0</b>	99.6±0.1	99.9±0.0	<b>100.0±0.0</b>	<b>100.0±0.0</b>
	SVHN-C(2.0)		<b>100.0±0.0</b>	<b>100.0±0.0</b>	26.7±0.6	58.0±0.2	<b>100.0±0.0</b>	<b>100.0±0.0</b>	58.2±0.2	60.2±0.8
CelebA	CIFAR10		<b>99.8±0.0</b>	<b>99.8±0.0</b>	1.0±0.1	30.8±0.0	<b>100.0±0.0</b>	<b>100.0±0.0</b>	0.0±0.0	30.7±0.0
	CIFAR100		<b>99.8±0.0</b>	<b>99.8±0.0</b>	2.0±0.2	30.8±0.0	<b>100.0±0.0</b>	<b>100.0±0.0</b>	0.0±0.0	30.7±0.0
	Imagenet32		<b>100.0±0.0</b>	<b>100.0±0.0</b>	87.9±0.3	90.5±0.1	<b>100.0±0.0</b>	<b>100.0±0.0</b>	96.7±0.4	97.4±0.2
	Imagenet32-C(0.07)		<b>100.0±0.0</b>	<b>100.0±0.0</b>	23.0±0.3	36.4±0.2	<b>100.0±0.0</b>	<b>100.0±0.0</b>	11.7±0.3	32.4±0.2
	SVHN		<b>100.0±0.0</b>	<b>100.0±0.0</b>	91.5±0.6	89.9±1.4	<b>100.0±0.0</b>	<b>100.0±0.0</b>	98.6±0.2	98.5±0.2
	SVHN-C(1.8)		<b>100.0±0.0</b>	<b>100.0±0.0</b>	1.4±0.2	30.8±0.0	<b>100.0±0.0</b>	<b>100.0±0.0</b>	0.0±0.0	30.7±0.0

Table 7 and 8 shows the experimental results using the model checkpoint released by OpenAI. Note that, since the model likelihood of CIFAR10 training split and test split do not fit very well<sup>9</sup>, so the performance of Ty-test on CIFAR10 vs SVHN degrades severely. The results in Table 7 is not fair for Ty-test. Our method is not affected by possible overfitting or underfitting.

In Table 9 to 13, we report more experimental results of DOCR- $\sigma$ -Corr. Compared with DOCR-TC, DOCR- $\sigma$ -Corr needs slightly larger batch size to achieve the same performance. Both CTR- $\sigma$ -Corr and CTR-TC are better than the state-of-the-art methods [35] and robust to data manipulation.

Table 14 shows the results of using  $p(\mathbf{z})$  for 1 vs rest classification on FashionMNIST with class conditional Glow. These results show that  $p(\mathbf{z})$  of class conditional Glow cannot be used for classification.

Table 15 shows the results of using reconstruction probability  $E_{z \sim q_\phi}[\log p_\theta(\mathbf{x}|\mathbf{z})]$  for OOD detection in VAE.

<sup>7</sup><https://github.com/y0ast/Glow-PyTorch>

<sup>8</sup><https://storage.googleapis.com/glow-demo/logs/abl-1x1-aff.tar>

<sup>9</sup>We did not search more hyperparameters due to resource limitation.

Table 7: Glow trained on CIFAR10, tested on other datasets, using checkpoint released by OpenAI. **EACH ROW** is for one **DATASET**.

Batch size	$m=10$				$m=25$			
Methods	DOCR-TC		Ty-test		DOCR-TC		Ty-test	
Metric	AUROC	AUPR	AUROC	AUPR	AUROC	AUPR	AUROC	AUPR
SVHN	<b>100.0±0.0</b>	<b>100.0±0.0</b>	59.6±0.2	52.2±0.3	<b>100.0±0.0</b>	<b>100.0±0.0</b>	64.4±0.4	56.4 ± 0.7
CelebA	<b>100.0±0.0</b>	<b>100.0±0.0</b>	<b>100.0±0.0</b>	<b>100.0±0.0</b>	<b>100.0±0.0</b>	<b>100.0±0.0</b>	<b>100.0±0.0</b>	<b>100.0±0.0</b>
Imagenet32	<b>100.0±0.0</b>	<b>100.0±0.0</b>	<b>100.0±0.0</b>	<b>100.0±0.0</b>	<b>100.0±0.0</b>	<b>100.0±0.0</b>	<b>100.0±0.0</b>	<b>100.0±0.0</b>

Table 8: Glow trained on CIFAR10, tested on CIFAR100, using checkpoint released by OpenAI. **EACH ROW** is for one **BATCH SIZE**. We are **the first** to solve CIFAR10 vs CIFAR100 problem on Glow.

Method	DOCR-TC		DOCR- $\sigma$ -Corr		Ty-test	
Metric	AUROC	AUPR	AUROC	AUPR	AUROC	AUPR
$m=25$	64.6±0.9	66.0±1.6	<b>77.3±1.4</b>	<b>78.2±1.5</b>	59.2±0.5	60.8±0.9
$m=50$	68.2±3.2	69.7±3.6	<b>85.9±1.3</b>	<b>86.9±1.0</b>	62.5±0.6	64.1±0.5
$m=75$	69.1±2.0	70.6±3.2	<b>91.3±1.9</b>	<b>91.9±1.9</b>	65.7±1.5	66.7±1.4
$m=100$	67.8±3.4	67.7±4.3	<b>93.6±1.8</b>	<b>94.1±1.9</b>	68.2±1.2	70.2±1.2
$m=125$	67.7±3.8	66.9±3.5	<b>96.2±1.4</b>	<b>96.3±1.6</b>	71.0±1.6	71.2±3.6
$m=150$	67.7±2.0	67.8±2.5	<b>98.2±0.9</b>	<b>98.4±0.8</b>	73.0±1.0	72.7±1.8
$m=175$	71.5±5.2	73.4±2.6	<b>98.0±1.0</b>	<b>98.0±1.1</b>	72.2±1.8	74.2±2.3
$m=200$	68.4±2.6	70.8±2.8	<b>98.9±1.0</b>	<b>99.1±0.7</b>	73.6±2.1	76.3±2.7

Table 9: Glow trained on FashionMNIST, tested on other datasets. **EACH ROW** is for one **DATASET**.

Method	DOCR- $\sigma$ -Corr			
Batch size	$m=10$		$m=25$	
Metric	AUROC	AUPR	AUROC	AUPR
MNIST	85.7±0.5	86.6±0.4	99.8±0.0	99.9±0.0
MNIST-C(10.0)	89.5±0.6	90.2±0.6	100.0±0.0	100.0±0.0
notMNIST	99.9±0.0	99.9±0.0	100.0±0.0	100.0±0.0
notMNIST-C(0.005)	95.5±0.3	96.3±0.2	100.0±0.0	100.0±0.0

Table 10: Glow trained on SVHN, tested on other datasets.

Method	DOCR- $\sigma$ -Corr			
Batch size	$m=10$		$m=25$	
Metric	AUROC	AUPR	AUROC	AUPR
CelebA	91.8±0.7	92.5±0.6	100.0±0.0	100.0±0.0
CelebA-C(0.08)	98.6±0.2	98.8±0.1	100.0±0.0	100.0±0.0
CIFAR10	87.8±0.7	88.8±0.7	99.2±0.2	99.3±0.2
CIFAR10-C(0.12)	89.4±0.5	90.1±0.4	99.7±0.0	99.7±0.0
CIFAR100	90.1±0.5	91.2±0.5	99.5±0.0	99.5±0.0
CIFAR100-C(0.12)	92.3±0.6	93.3±0.5	99.8±0.0	99.8±0.0
Imagenet32	88.9±0.5	90.0±0.5	99.4±0.2	99.4±0.2
Imagenet23-C(0.07)	97.4±0.3	97.8±0.2	100.0±0.0	100.0±0.0

Table 11: Glow trained on CIFAR10, tested on other datasets.

Method	DOCR- $\sigma$ -Corr			
Batch size	$m=10$		$m=25$	
Metric	AUROC	AUPR	AUROC	AUPR
SVHN	83.3±0.7	83.3±0.5	99.7±0.1	99.7±0.0
CelebA	87.7±0.1	88.2±0.4	100.0±0.0	100.0±0.0
Imagenet32	75.1±0.5	76.6±0.6	92.5±1.0	93.4±0.8

Table 12: Glow trained on SVHN, tested on other datasets.

Method	DOCR- $\sigma$ -Corr			
Batch size	$m=10$		$m=25$	
Metric	AUROC	AUPR	AUROC	AUPR
MNIST	100.0 $\pm$ 0.0	100.0 $\pm$ 0.0	100.0 $\pm$ 0.0	100.0 $\pm$ 0.0
notMNIST	100.0 $\pm$ 0.0	100.0 $\pm$ 0.0	100.0 $\pm$ 0.0	100.0 $\pm$ 0.0
CelebA	91.8 $\pm$ 0.7	92.5 $\pm$ 0.6	100.0 $\pm$ 0.0	100.0 $\pm$ 0.0
Imagenet32	88.9 $\pm$ 0.5	90.0 $\pm$ 0.5	99.4 $\pm$ 0.2	99.4 $\pm$ 0.2
CIFAR10	87.8 $\pm$ 0.7	88.8 $\pm$ 0.7	99.2 $\pm$ 0.2	99.3 $\pm$ 0.2
CIFAR100	90.1 $\pm$ 0.5	91.1 $\pm$ 0.5	99.5 $\pm$ 0.0	99.5 $\pm$ 0.0

Table 13: Glow trained on CelebA32, tested on other datasets.

Method	DOCR- $\sigma$ -Corr							
Batch size	$m=10$		$m=25$		$m=50$		$m=75$	
Metric	AUROC	AUPR	AUROC	AUPR	AUROC	AUPR	AUROC	AUPR
CIFAR10	53.6 $\pm$ 1.1	52.1 $\pm$ 0.7	66.3 $\pm$ 0.8	63.4 $\pm$ 1.2	86.9 $\pm$ 0.8	86.2 $\pm$ 1.7	96.7 $\pm$ 0.5	96.8 $\pm$ 0.5
CIFAR100	60.0 $\pm$ 0.8	59.1 $\pm$ 0.4	75.7 $\pm$ 0.8	73.7 $\pm$ 1.2	92.7 $\pm$ 1.0	92.6 $\pm$ 1.0	98.5 $\pm$ 0.6	98.2 $\pm$ 1.4
Imagenet32	75.8 $\pm$ 0.8	76.8 $\pm$ 0.9	90.8 $\pm$ 1.2	90.8 $\pm$ 0.9	98.5 $\pm$ 0.5	98.4 $\pm$ 0.7	99.8 $\pm$ 0.1	99.8 $\pm$ 0.1
Imagenet32-C(0.07)	65.7 $\pm$ 0.6	65.0 $\pm$ 1.0	82.7 $\pm$ 1.6	81.5 $\pm$ 1.4	96.3 $\pm$ 0.6	96.2 $\pm$ 0.7	99.6 $\pm$ 0.0	99.6 $\pm$ 0.0
SVHN	65.6 $\pm$ 1.2	63.6 $\pm$ 0.8	95.2 $\pm$ 0.8	94.8 $\pm$ 0.9	100.0 $\pm$ 0.0	100.0 $\pm$ 0.0	100.0 $\pm$ 0.0	100.0 $\pm$ 0.0
SVHN-C(1.8)	77.8 $\pm$ 1.0	76.6 $\pm$ 1.2	97.5 $\pm$ 0.2	97.0 $\pm$ 0.5	100.0 $\pm$ 0.0	100.0 $\pm$ 0.0	100.0 $\pm$ 0.0	100.0 $\pm$ 0.0

Table 14: Class conditional Glow trained on FashionMNIST. Use  $p(\mathbf{z})$  as criterion for 1 vs rest classification.

Method	$p(\mathbf{z})$	
Metrics	AUROC	AUPR
class 0 vs rest	72.7 $\pm$ 1.6	72.0 $\pm$ 1.4
class 1 vs rest	85.1 $\pm$ 0.6	86.2 $\pm$ 0.6
class 2 vs rest	74.8 $\pm$ 4.5	76.9 $\pm$ 4.0
class 3 vs rest	68.9 $\pm$ 4.7	71.2 $\pm$ 4.5
class 4 vs rest	77.1 $\pm$ 2.1	78.4 $\pm$ 3.2
class 5 vs rest	71.7 $\pm$ 1.4	71.9 $\pm$ 1.2
class 6 vs rest	73.5 $\pm$ 7.8	73.7 $\pm$ 8.6
class 7 vs rest	86.9 $\pm$ 0.4	88.6 $\pm$ 0.4
class 8 vs rest	55.5 $\pm$ 0.9	53.8 $\pm$ 0.5
class 9 vs rest	86.6 $\pm$ 0.3	87.1 $\pm$ 0.3

Table 15: VAE trained on CIFAR10. Use reconstruction probability for OOD data detection.

Method	reconstruction probability	
Metrics	AUROC	AUPR
SVHN	17.6 $\pm$ 0.0	34.3 $\pm$ 0.0
CelebA	83.1 $\pm$ 0.0	82.5 $\pm$ 0.0
Imagenet32	72.4 $\pm$ 0.2	75.0 $\pm$ 0.1
CIFAR100	52.3 $\pm$ 0.0	53.6 $\pm$ 0.0



## C More Figures

In this section, we list out more figures. The captions are self-explanatory.

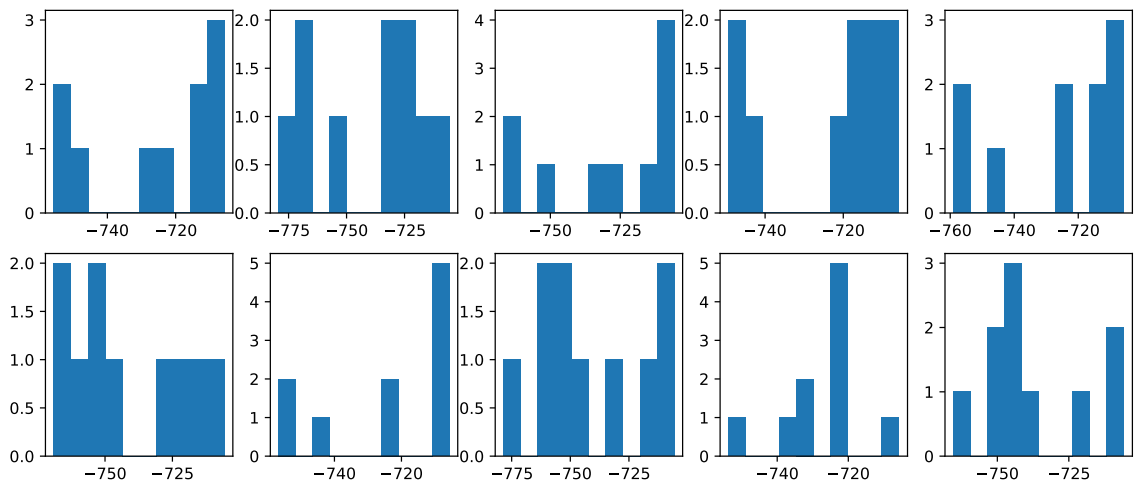


Figure 7: We train class conditional Glow on FashionMNIST. The log-probabilities of 10 centroids under each Gaussian are close to  $768 \times \log(1/\sqrt{2\pi}) \approx -705.74$ , which is the log-probability of the center of 768-dimensional isotropic Gaussian. These results demonstrate that the centroids are close to each other.

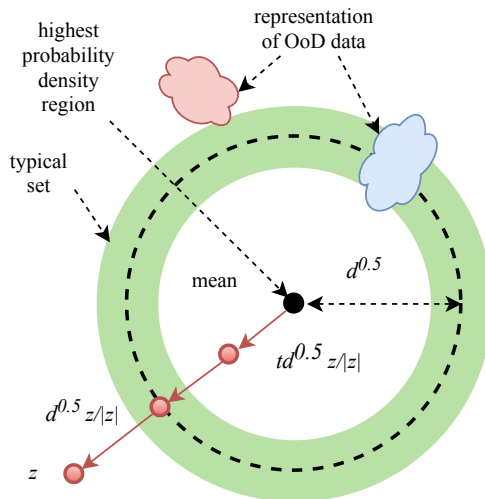
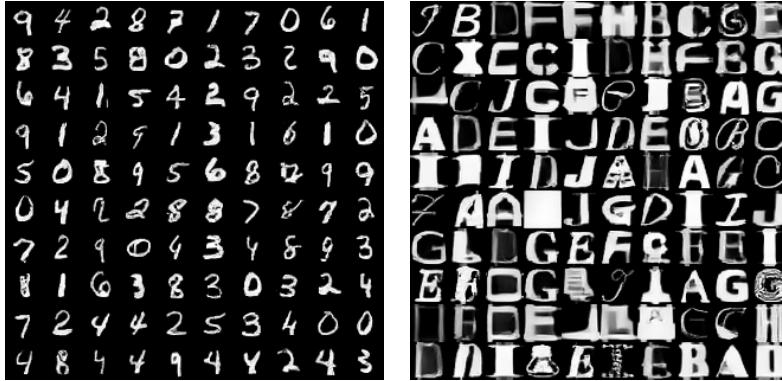
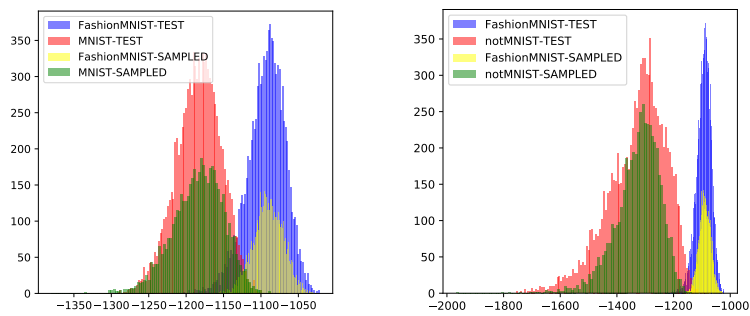


Figure 8: Typical set of  $d$ -dimensional isotropic Gaussian is an annulus with radius  $\sqrt{d}$ . We can scale any point  $z$  to the typical set by multiplying a scalar  $\sqrt{d}/|z|$ . The representations of OoD data may reside in the typical set.



(a) MNIST from scaled representations (b) notMNIST from scaled representations

Figure 9: Attack on  $\log p(z)$ . Train Glow on FashionMNIST and test on MNIST and notMNIST. We scale the representations of OOD dataset to the typical set of prior Gaussian. The scaled latent vectors still corresponds to clear (a) hand-written digits or (b) letters. These results demonstrate that the typical set of prior may include the representations of OOD data, although these data are not included in the raw OOD dataset.



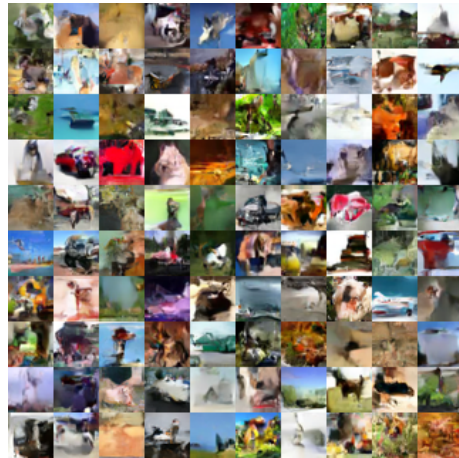
(a) FashionMNIST vs MNIST

(b) FashionMNIST vs notMNIST

Figure 10: Glow trained on FashionMNIST. Histogram of  $\log p(z)$  of (a) FashionMNIST vs MNIST, (b) FashionMNIST vs notMNIST under Glow. The green part corresponds to the  $\log p(z)$  of noises sampled from the fitted Gaussian of OOD datasets.



(a)



(b)



(c)



(d)



(e)

Figure 11: Glow trained on CIFAR10. Generated images according to the fitted Gaussian from representations of (a) MNIST; (b) CIFAR100; (c) SVHN; (d) Imagenet32; (e) CelebA. We replicate MNIST into three channels and pad zeros for consistency. These results demonstrate that the covariance of representations contains important information of an OOD dataset.

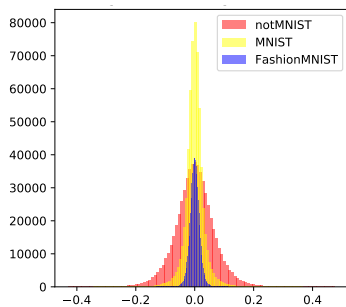


Figure 12: Glow trained on FashionMNIST, tested on MNIST/notMNIST. Non-diagonal elements in correlation of representations of OOD datasets are more divergent from zero.



Figure 13: Glow trained on FashionMNIST. Sampling according to prior (up), fitted Gaussian from representations of MNSIT (middle) and notMNIST (down).

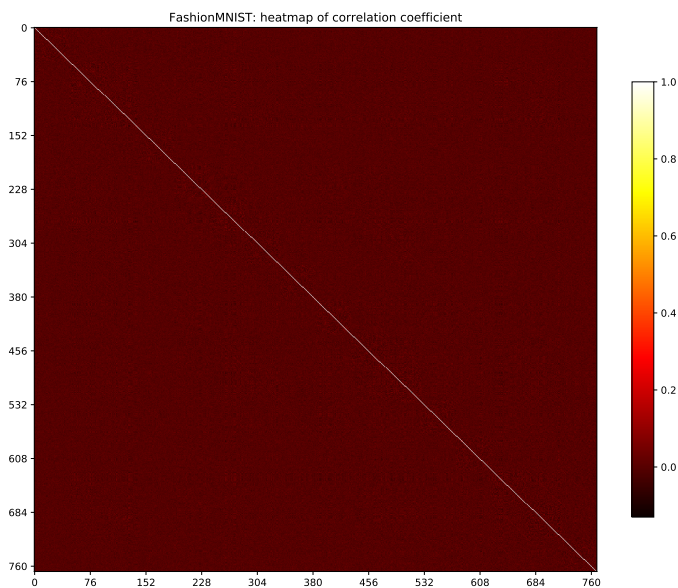


Figure 14: Glow trained on FashionMNIST. Heatmap of correlation of FashionMNIST representations.

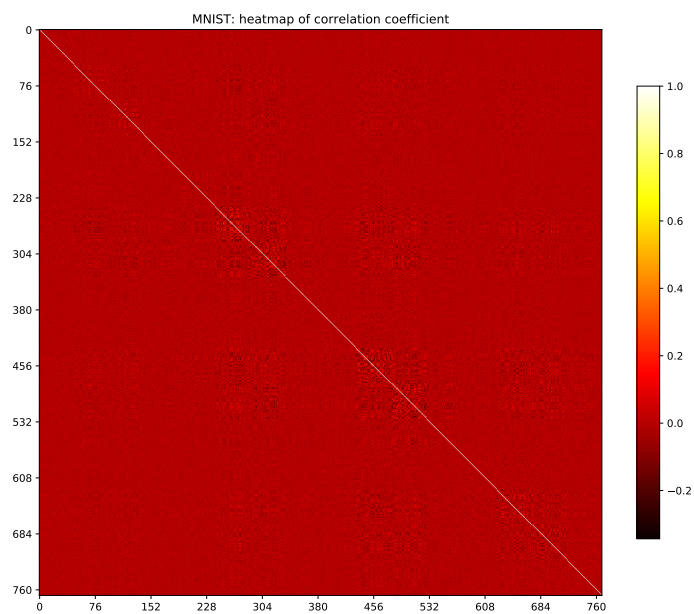


Figure 15: Glow trained on FashionMNIST. Heatmap of correlation of MNIST representations.

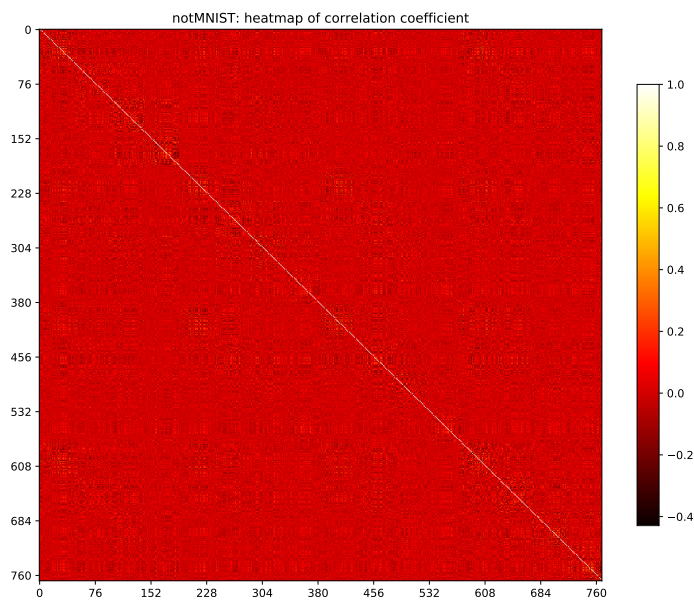


Figure 16: Glow trained on FashionMNIST. Heatmap of correlation of notMNIST representations.

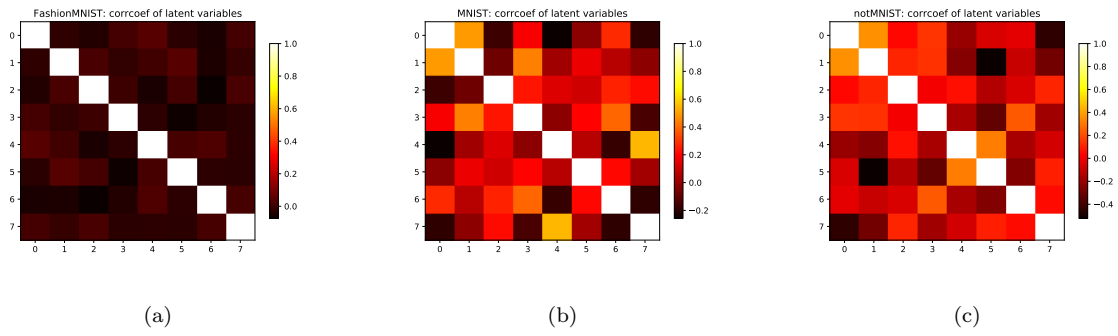


Figure 17: VAE trained on FashionMNIST. Heatmap of correlation of (a) FashionMNIST (b) MNIST (c) notMNIST representations.

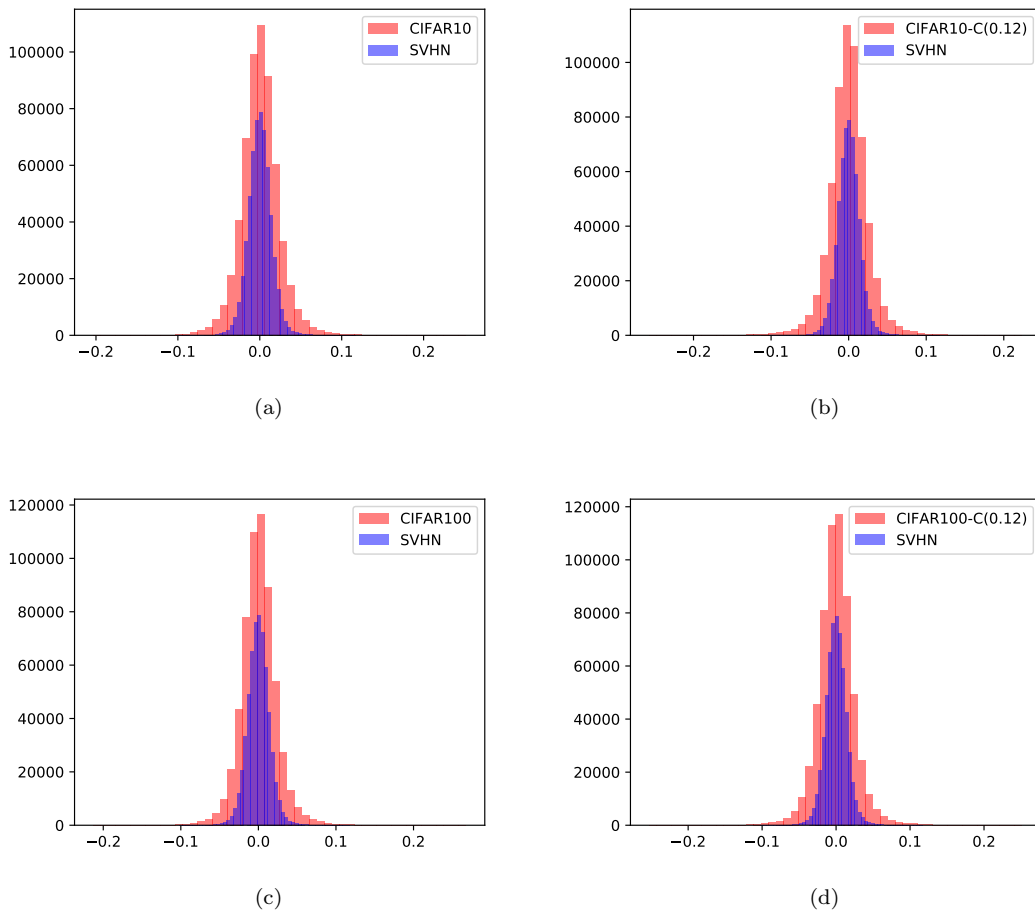


Figure 18: Glow trained on SVHN. Histogram of non-diagonal elements of correlation of representations.



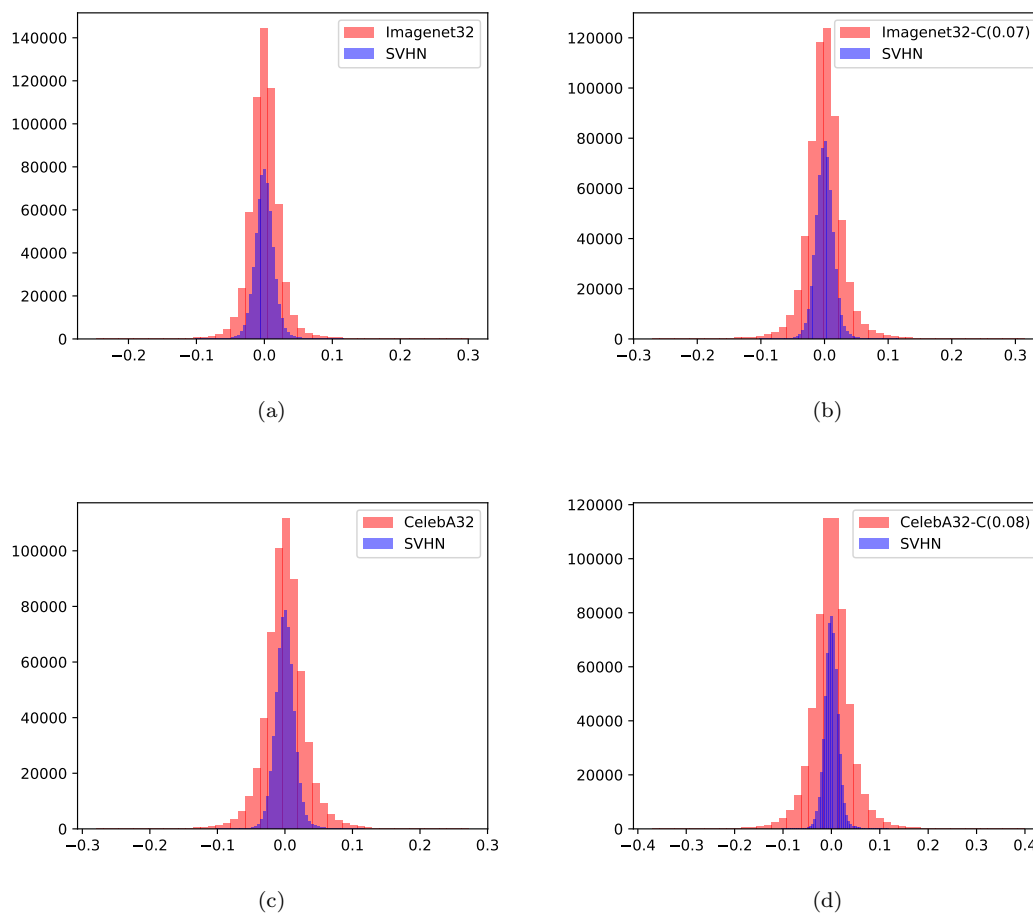


Figure 19: Glow trained on SVHN. Histogram of non-diagonal elements of correlation of representations.

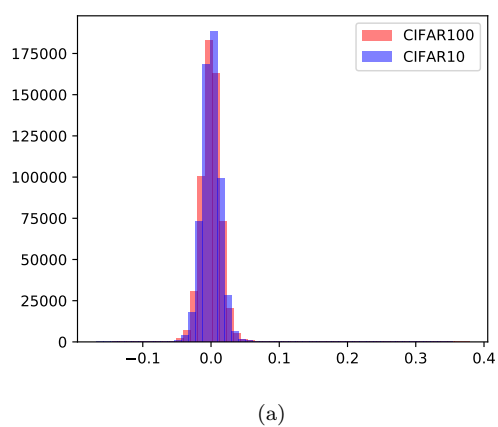


Figure 20: Glow trained on CIFAR10. Histogram of non-diagonal elements of correlation of representations.



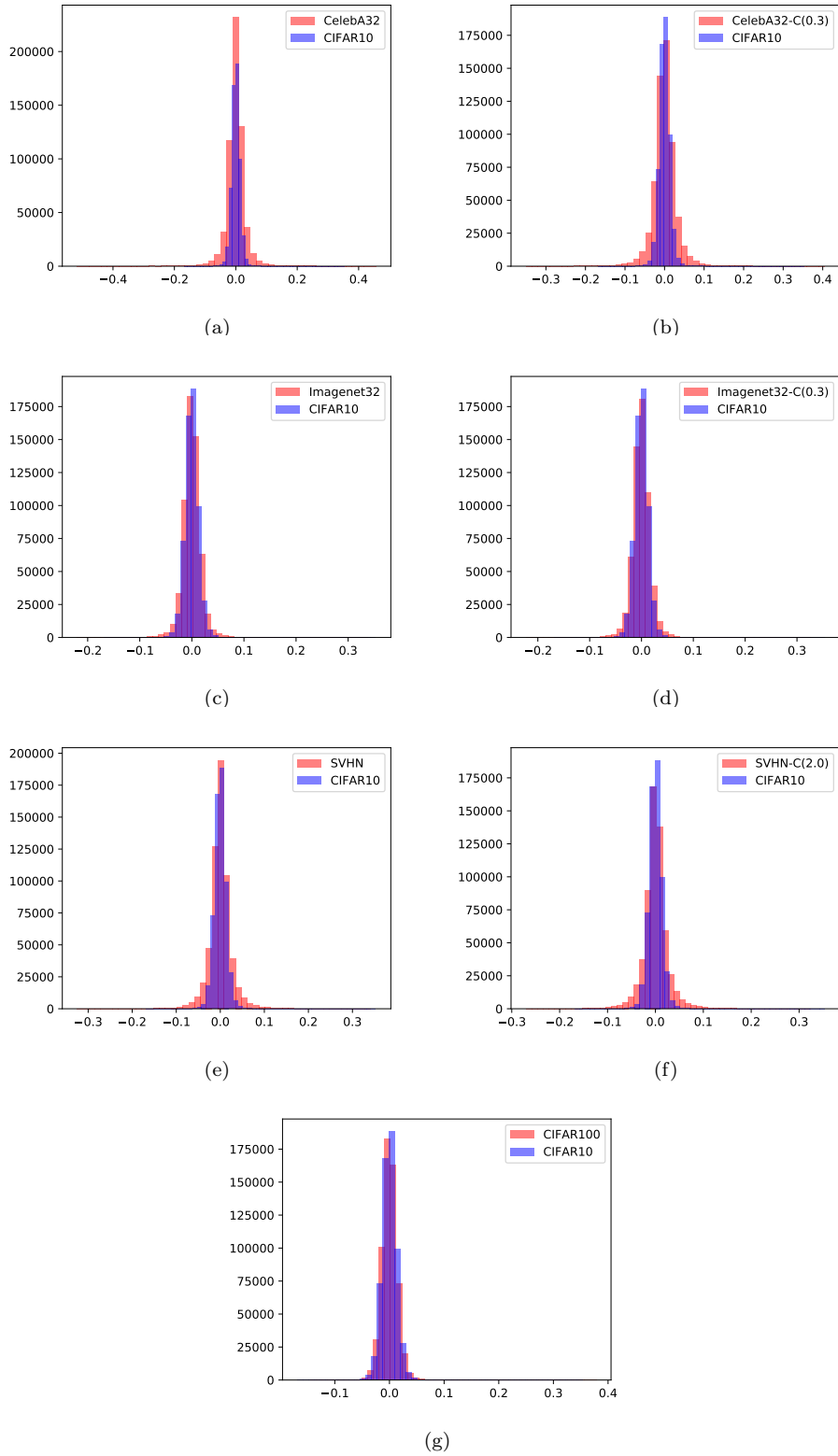
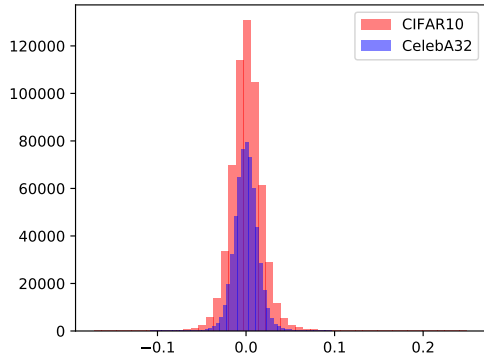
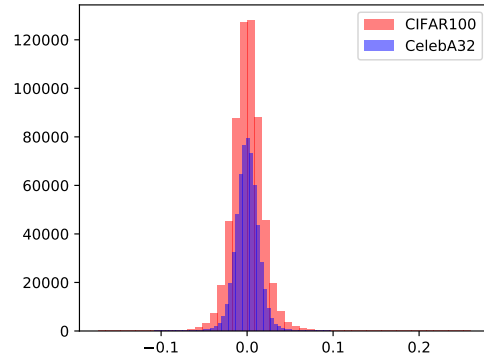


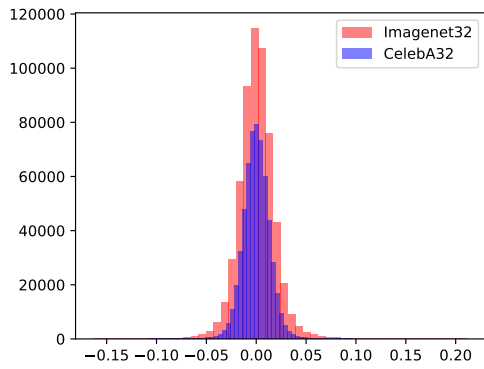
Figure 21: Glow trained on CIFAR10. Histogram of non-diagonal elements of correlation of representations.



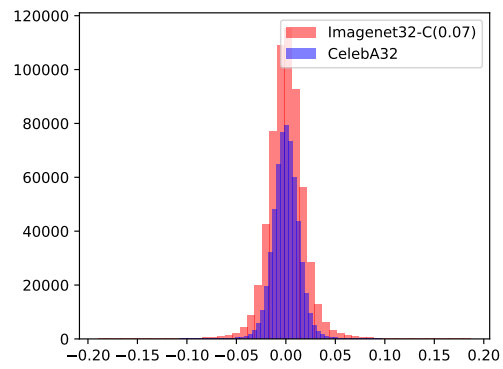
(a)



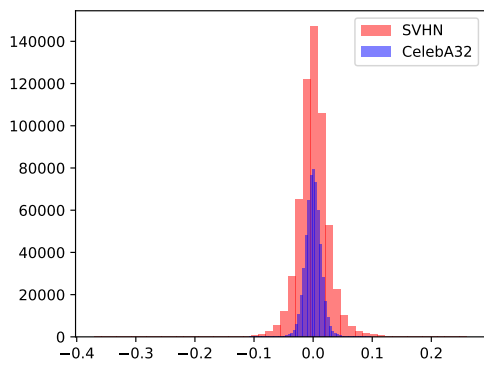
(b)



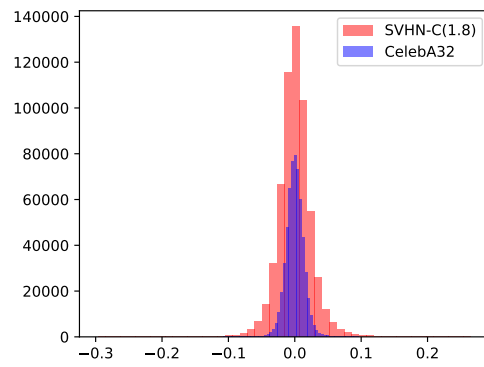
(c)



(d)



(e)



(f)

Figure 22: Glow trained on CelebA. Histogram of non-diagonal elements of correlation of representations.

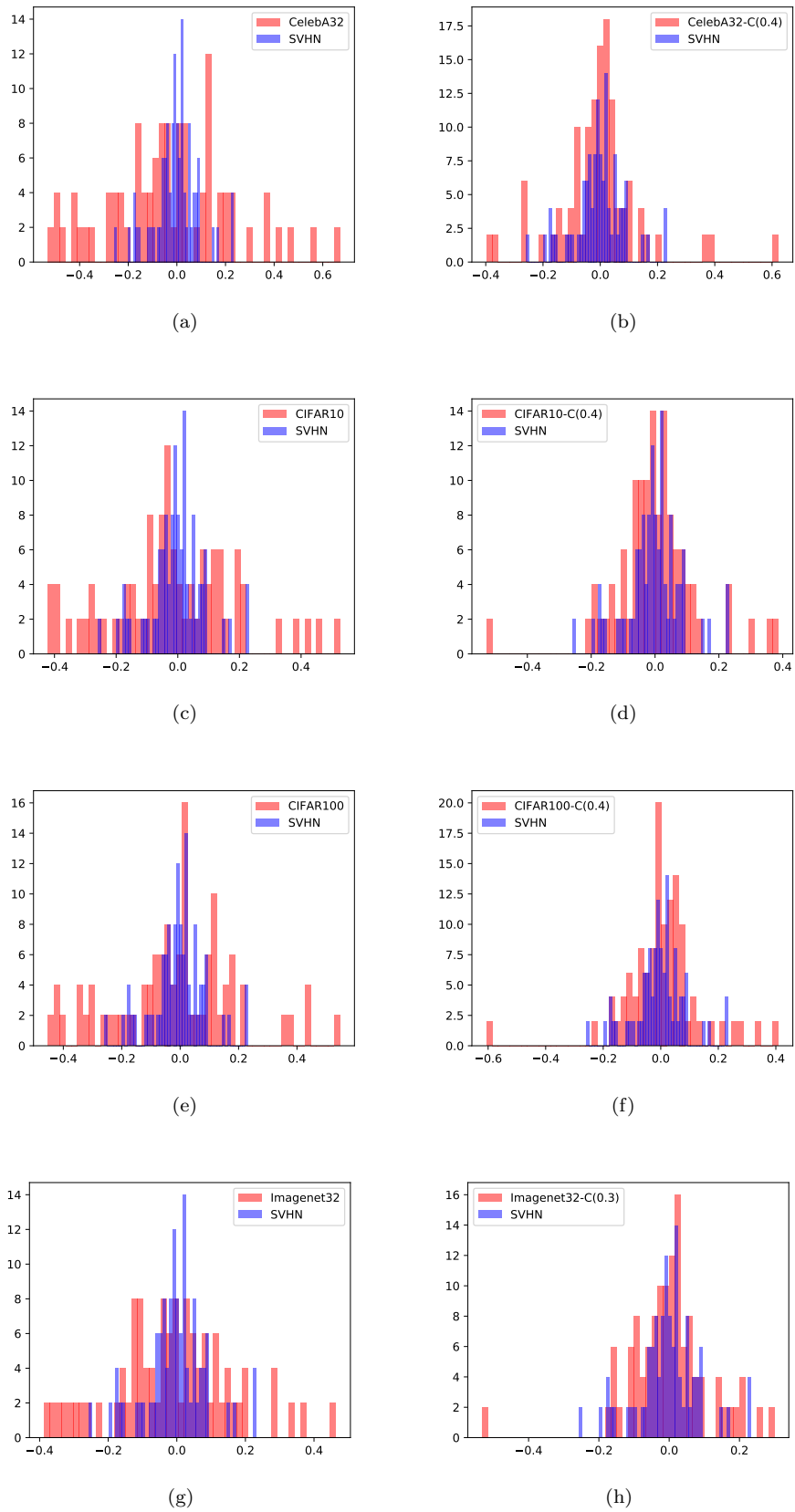


Figure 23: VAE trained on SVHN. Histogram of non-diagonal elements of correlation of sampled representations.

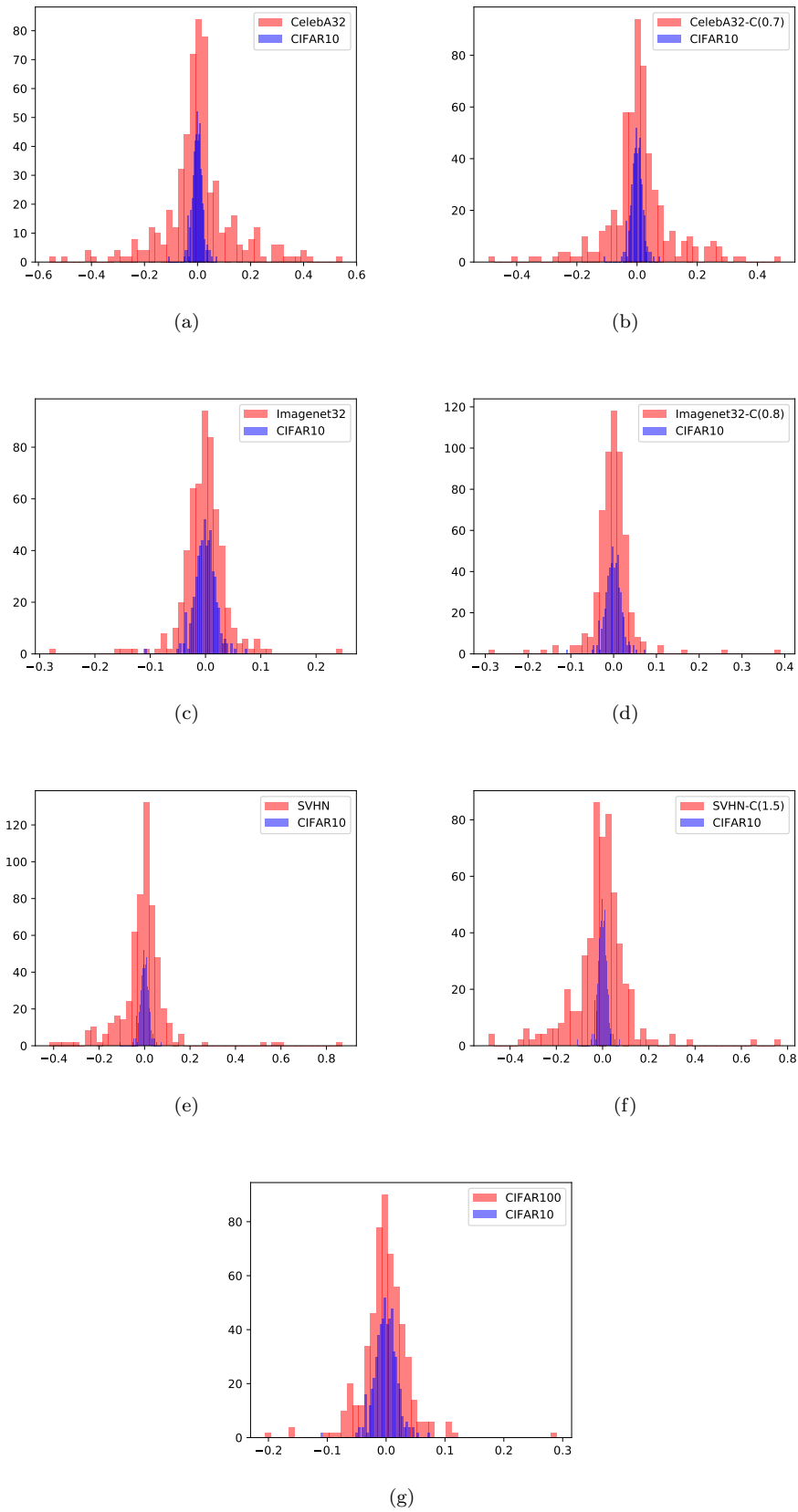
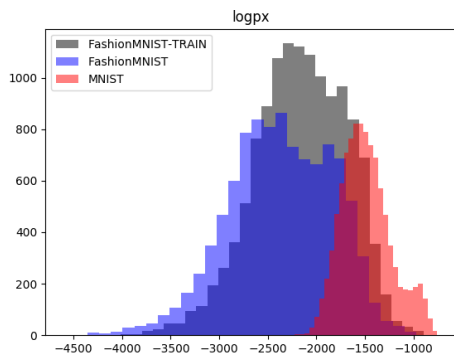
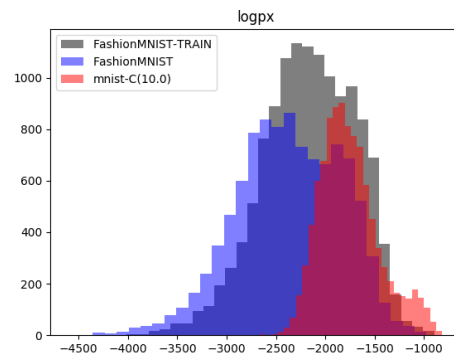


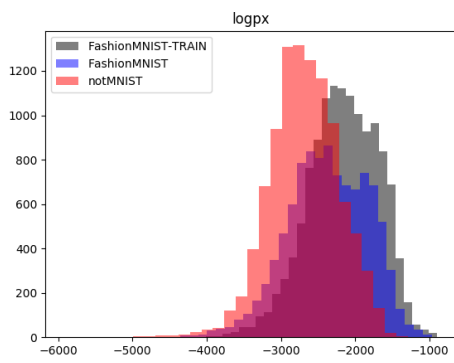
Figure 24: VAE trained on CIFAR10. Histogram of non-diagonal elements of correlation of sampled representations.



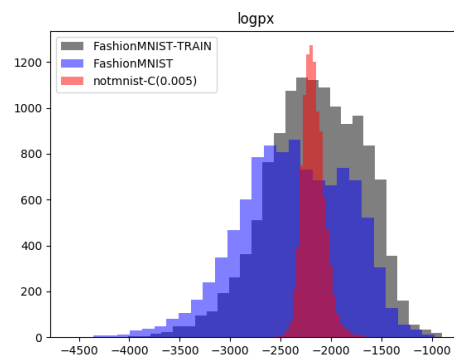
(a)



(b)

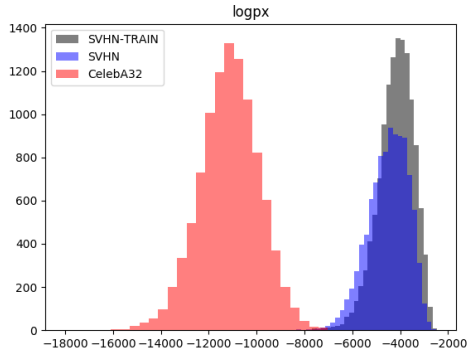


(c)

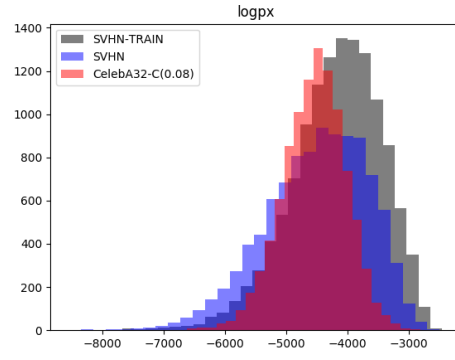


(d)

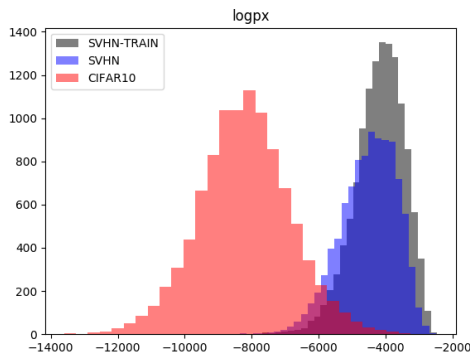
Figure 25: Glow trained on FashionMNIST. Histogram of  $\log p(\mathbf{x})$ .



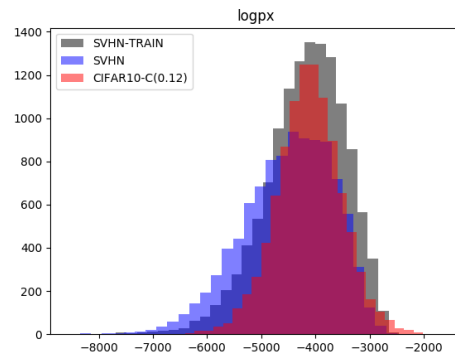
(a)



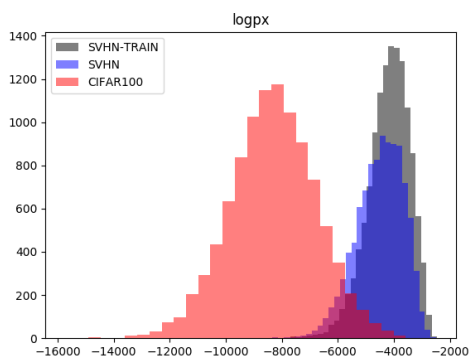
(b)



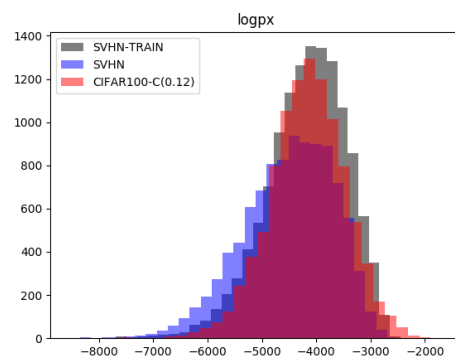
(c)



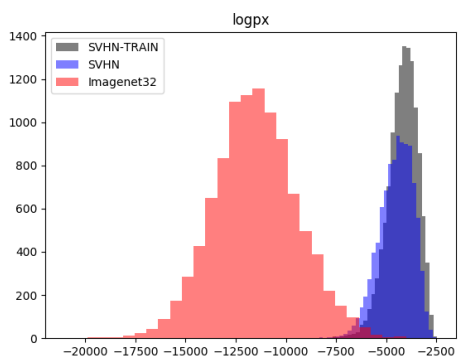
(d)



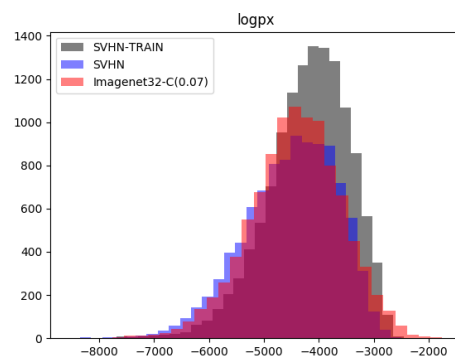
(e)



(f)

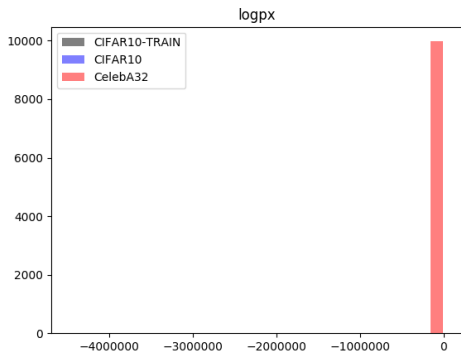


(g)

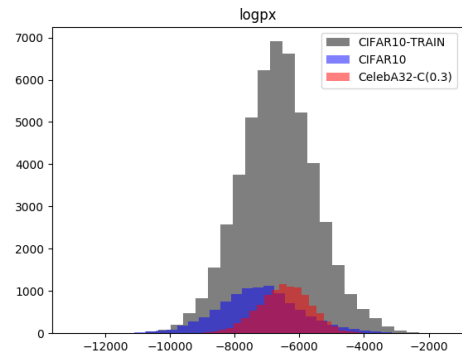


(h)

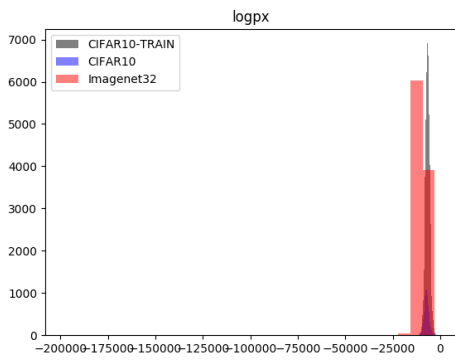
Figure 26: Glow trained on SVHN. Histogram of  $\log p(\mathbf{x})$ .



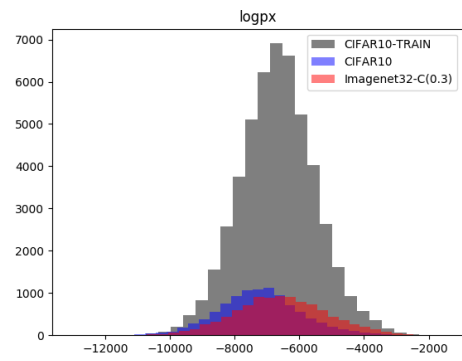
(a)



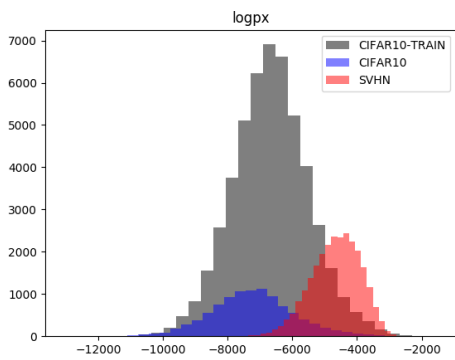
(b)



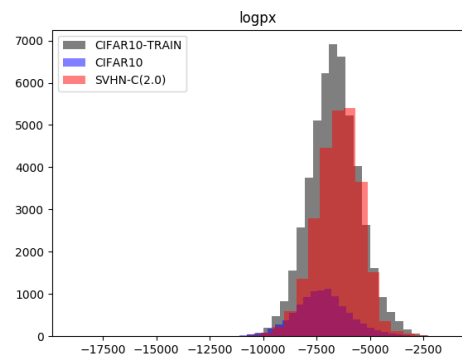
(c)



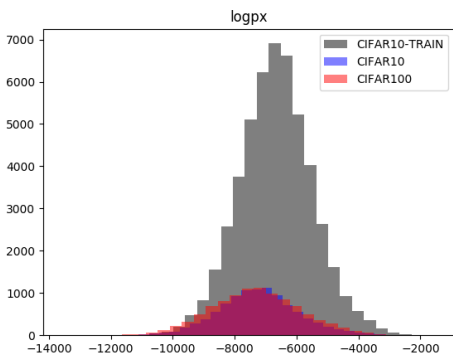
(d)



(e)



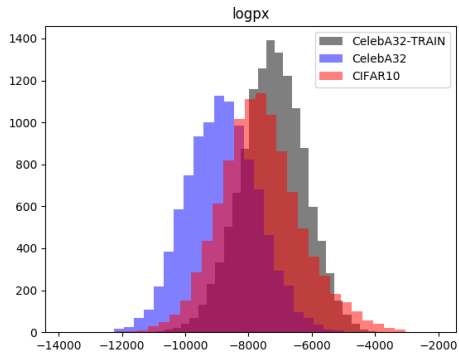
(f)



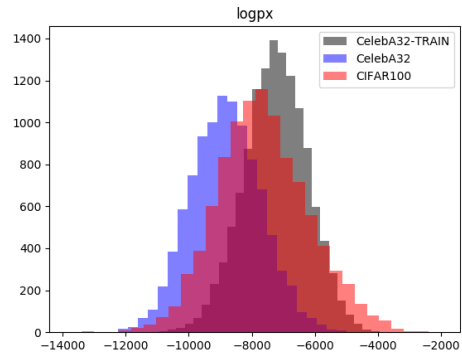
(g)

Figure 27: Glow trained on CIFAR10. Histogram of  $\log p(\mathbf{x})$ . For CIFAR10 vs CelebA, the range of  $\log p(\mathbf{x})$  of CelebA is too large such that the  $x$ -axis scale is distorted.

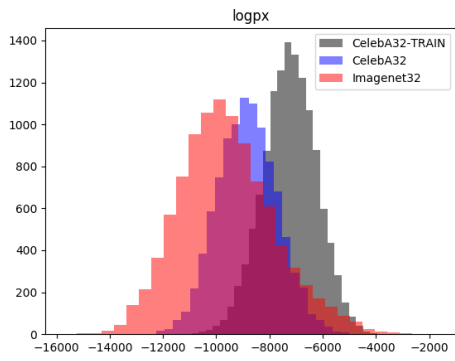




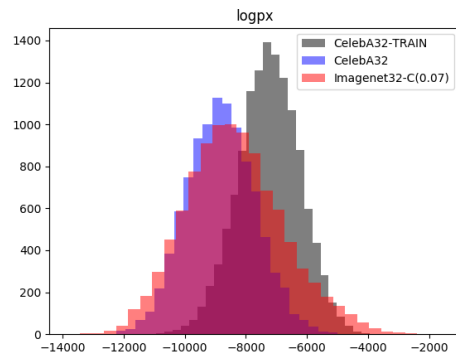
(a)



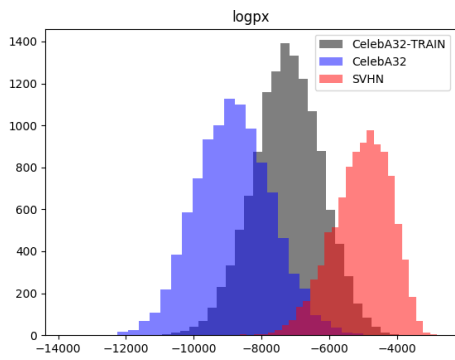
(b)



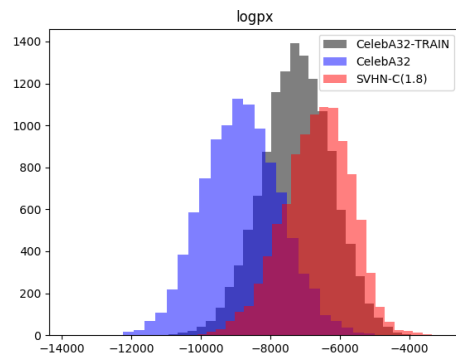
(c)



(d)



(e)

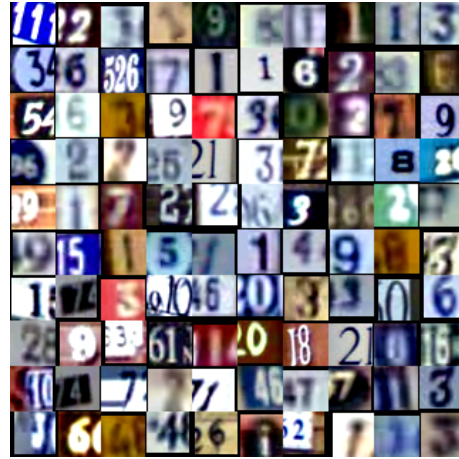


(f)

Figure 28: Glow trained on CelebA. Histogram of  $\log p(\mathbf{x})$ .



(a) SVHN



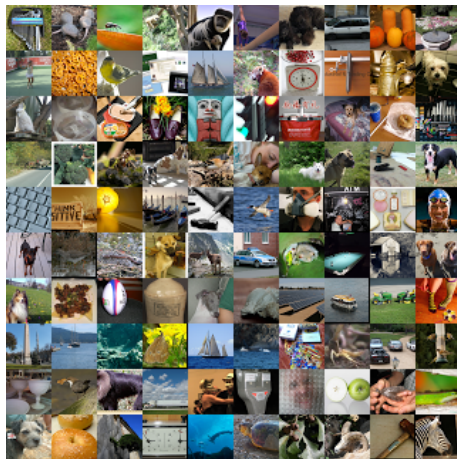
(b) SVHN with increased contrast by a factor of 2, have lower likelihood



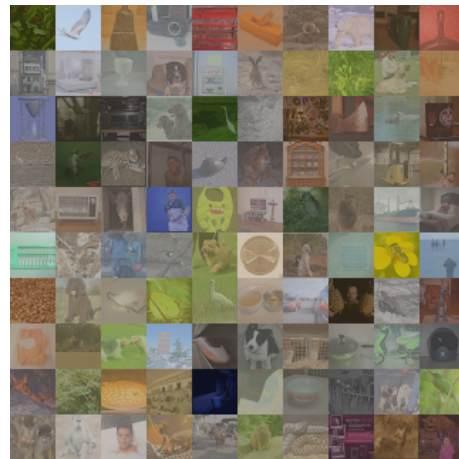
(c) CelebA32



(d) CelebA32 with decreased contrast by a factor of 0.3, have higher likelihood

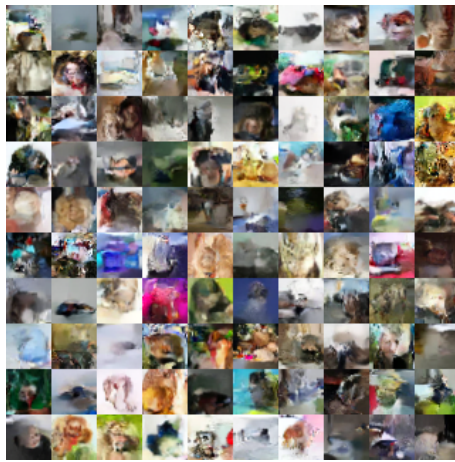
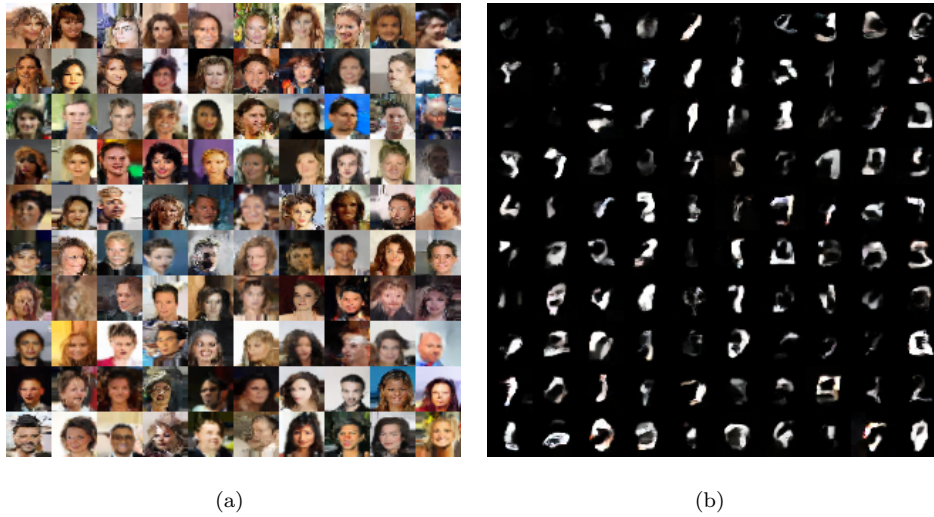


(e) Imagenet32



(f) Imagenet32 with decreased contrast by a factor of 0.3, have higher likelihood

Figure 29: Examples of datasets and their mutations. Under Glow trained on CIFAR10, these mutated datasets have the similar likelihood distribution with CIFAR10 test split.



(c)

Figure 30: Glow trained on CelebA $32 \times 32$ , sampling according to (a) isotropic Gaussian; (b) fitted Gaussian from MNIST representations; (c) fitted Gaussian from CIFAR10 representations.

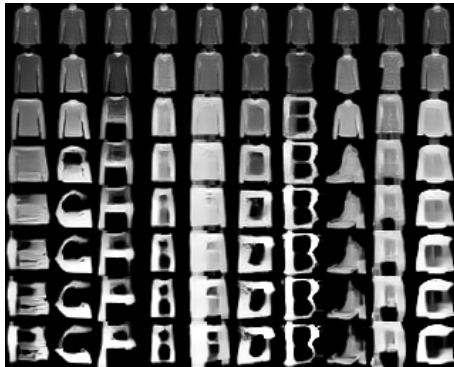


Figure 31: Glow trained on FashionMNIST, sampling according to covariance of notMNIST representations. For each row, we use a different temperature (0, 0.25, 0.5, 0.6, 0.7, 0.8, 0.9, 1.0). Images vary from clothes to letters with the increase of the temperature.

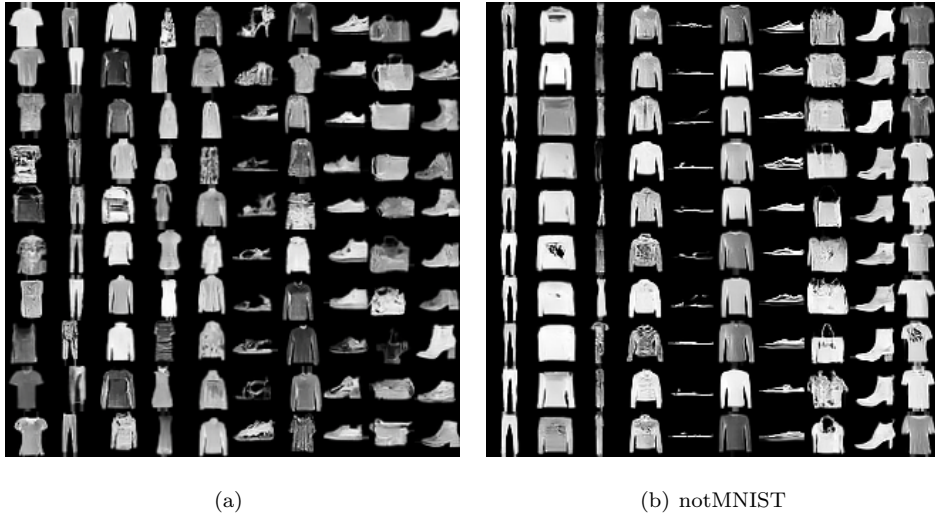


Figure 32: Class conditional Glow with 10 Gaussians on FashionMNIST. (a) sampling  $\epsilon \sim \mathcal{N}(\boldsymbol{\mu}_i, \text{diag}(\boldsymbol{\sigma}_i^2))$  for  $0 \leq i \leq 9$  and generate images  $f^{-1}(\epsilon)$ . The  $i$ -th column corresponds to Gaussian  $\mathcal{N}_i$ . (b) For the  $i$ -th Gaussian  $\mathcal{N}_i$ , we compute the normalized representations of the  $((i + 1)\%10)$ -th class input under  $\mathcal{N}_i$ , and compute the mean  $\boldsymbol{\mu}_{i'}$  and covariance  $\boldsymbol{\Sigma}_{i'}$ . Then we sample  $\epsilon_{i'} \sim \mathcal{N}(\boldsymbol{\mu}_{i'}, \boldsymbol{\Sigma}_{i'})$ , and compute  $f^{-1}(\epsilon_{i'} \cdot \boldsymbol{\sigma}_i + \boldsymbol{\mu}_i)$  to generate new images. The  $i$ -th column is from  $\epsilon_{i'}$ . we can generate almost high quality images of the  $((i + 1)\%10)$ -th class from the fitted Gaussian. But we notice that the images are not varied as like that sampled from prior.